Memo version 2.0

BESIII Analysis Memo

DocDB-735

BAM-357

May 8, 2021

The Study of $D_s^+ \to K^+K^-e^+\nu_e$

Shu-Lei Zhang[a,b], Liao-Yuan Dong[a], and Yuan-Ning Gao[c]

[a]*Hunan University*
[b]*Institute of High Energy Physics, CAS*
[c]*Tsinghua University*

Internal Referee Committee

Ref1 Hailong Ma (Chair)[c], Ref2 Minggang Zhao[d], and Ref3 Longke Li[c]

[c]*Institue of High Energy Physics, CAS*
[d]*Nankai University*

DocDB : http://docbes3.ihep.ac.cn/cgi-bin/DocDB/ShowDocument?docid=735

Hypernews : http://hnbes3.ihep.ac.cn/HyperNews/get/paper357.html

Abstract

Using 3.19 fb^{-1} of data recorded by the BESIII detector at $\sqrt{s} = 4.178$ GeV, we present an analysis of $D_s^+ \to K^+K^-e^+\nu_e$ decay channel. The absolute branching fraction of $D_s^+ \to \phi e^+\nu_e$ is measured to be $\mathcal{B}(D_s^+ \to \phi e^+\nu_e) = (2.31 \pm 0.10 \pm 0.09) \times 10^{-2}$. By performing a fit to the five-dimensional decay distributions, we extract the hadronic form factor ratios of $D_s^+ \to \phi e^+\nu_e$ at $q^2 = 0$ assuming single-pole dominance parameterization: $r_V = \frac{V(0)}{A_1(0)} = 1.31 \pm 0.16 \pm 0.06$, $r_2 = \frac{A_2(0)}{A_1(0)} = 0.76 \pm 0.17 \pm 0.05$. In these values, the first errors are statistical and the second systematic. We also search for a possible S-wave contribtution from $f_0(980) \to K^+K^-$, but no significant excess is found.

Contents

1 Introduction

The semileptonic decay of charm meson is important for studying the strong and weak interactions. It can be used to test techniques developed for solving perturbative and non-perturbative problems in quantum chromodynamics (QCD), and to extract elements of the Cabibbo-Kobayashi-Maskawa (CKM) matrix [1], which parameterizes the mixing between the quark mass eigenstates. One important task in the field of flavor physics is to over-constrain the CKM matrix, which strictly satisfies unitarity in the Standard Model (SM) of particle physics. By measuring these matrix elements precisely, we will understand better the SM physics and test it. Especially, it gives us the opportunity to discover new physics since any deviation from prediction by the unitary requirement indicates some new mechanism beyond the SM.

However, the extraction of the CKM matrix elements is difficult because quarks are bound inside hadrons by the strong interaction. Semileptonic decay is simpler than hadronic decay of the charm meson because leptons do not involve the strong interaction. The decay amplitude is proportional to the product of the CKM matrix element and the hadronic form factor. The latter describes the strong interaction between quarks in the final state. The form factors include all the non-perturbative effects. Several methods can be used to treat these problems, such as quark model (QM) [2], lattice QCD (LQCD) [3], and QCD sum rule (QCDSR) [4], among which LQCD and QCDSR are based on first principles of QCD. Combined with the measured decay rate from experimental data and the hadronic form factors from theoretical calculation, we have the opportunity to extract the CKM matrix element, and vice versa, the theoretical calculation for the form factors can be checked when the precise CKM matrix element and the decay rate are used. So the inputs from experimental data and theoretical calculations are both important.

In the charm sector, due to the quite precise $|V_{cs}|$ value, the semileptonic decay $D_s^+ \to \phi e^+ \nu_e$ provides an excellent testing ground for different calculations about the hadronic form factors and its decay branching fraction. The feynman diagram of this decay is shown in Fig. 1 (Charge conjugate reactions are always implied throughout this document). It is well suited to study the hadronic form factors because the ϕ meson is a narrow resonance which can be well isolated experimentally. The hadronic form factors were calculated theoretically by LQCD [5, 6, 7], QCDSR [8], and a relativistic quark model in the covariant light-front approach (CLF) [9, 10, 11, 12]. Using limits of large energy effective theory and heavy quark effective theory (HQET), Ref. [13] provides the theorectial precdictions for the form factors and the branching fraction. With the help of a chiral unitarity approach (CUA) in coupled channels, Ref. [14] computes the branching fraction. In addition, Refs. [11, 12] also predict this branching fraction using the covariant light-front approach. These different theoretical calculations and comparisons

with experimental measurements are summaried in Table 1. In the summary, we compare them with our measurement and make a discussion.

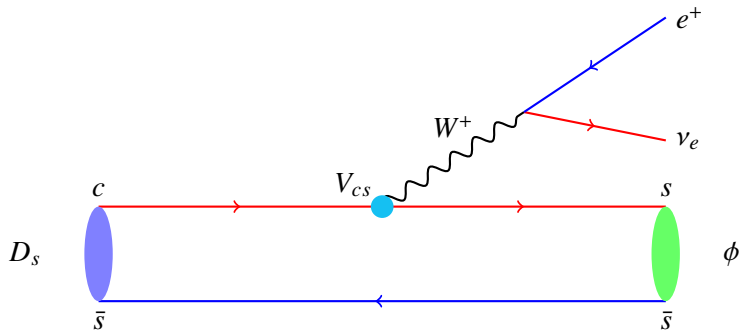

Figure 1: Feynman diagram of semileptonic decay $D_s^+ \to \phi e^+ \nu_e$

Table 1: Form factors and branching fraction of $D_s \to \phi$ transition from different theoretical calculations and comparisons with experimental measurements. Here $r_V = V(0)/A_1(0)$ and $r_2 = A_2(0)/A_1(0)$.

Refs.	V(0)/r_V	$A_0(0)$	$A_1(0)$	$A_2(0)/r_2$	$\mathcal{B}(D_s^+ \to \phi e^+ \nu_e)(\%)$
LQCD [5]	$1.30\pm0.32 \pm 0.43/2.00\pm0.19^{+0.20}_{-0.25}$	$0.71\pm0.13 \pm 0.23$	$0.73\pm0.12 \pm 0.24$	$0.55\pm0.10^{+0.24}_{-0.20}/0.78\pm0.08^{+0.17}_{-0.13}$	–
LQCD [6]	$1.36\pm0.04/2.01\pm0.04$	0.80 ± 0.02	0.67 ± 0.01	$0.47\pm0.06/0.68\pm0.07$	–
LQCD [7]	$1.059\pm0.124/1.72\pm0.21$	0.706 ± 0.037	0.615 ± 0.024	$0.457\pm0.078/0.74\pm0.12$	–
QCDSR [8]	$1.21\pm0.33/2.20\pm0.85$	0.42 ± 0.12	0.55 ± 0.15	$0.59\pm0.17/1.07\pm0.43$	1.8 ± 0.5
CLF [9]	–/1.569	–	–	–/0.865	–
CLF [10, 11]	–/1.42	–	–	–/0.86	3.1 ± 0.3
CLF [12]	–/1.49	–	–	–/0.95	2.3
HQET [13]	1.10/1.80	1.02	0.61	0.32/0.52	2.4
CUA [14]	–	–	–	–	2.12
BABAR [15] (Exp.)	$-/1.807\pm0.046\pm0.065$	–	$0.607\pm0.011\pm0.019\pm0.018$	$-/0.816\pm0.036\pm0.030$	$2.61 \pm 0.03 \pm 0.08 \pm 0.15$
CLEO [16] (Exp.)	–	–	–	–	$2.36 \pm 0.23 \pm 0.13$
CLEO [17] (Exp.)	–	–	–	–	$2.14 \pm 0.17 \pm 0.08$
FOCUS [18] (Exp.)	$-/1.549\pm0.250\pm0.148$	–	–	$-/0.713\pm0.202\pm0.284$	–

2 Analytic Strategy of Branching Fraction Measurement

The data sample for this analysis is collected at $E_{\rm cm}$= 4.178 GeV, about 100 MeV higher than $D_s^* D_s$ threshold. Around this energy region, based on the cross section measurement by CLEO [19], we know that most D_s production in e^+e^- collision comes from $D_s^{*\pm}D_s^{\mp}$ events with its cross section approximately 0.9 nb, while the cross section for $D_s^+D_s^-$ is about a factor of 20 smaller. The D_s^* decays to either γD_s or $\pi^0 D_s$ with branching fractions of $(93.5 \pm 0.7)\%$ and $(5.8 \pm 0.7)\%$ [20], respectively. The other charm productions total $\sim$ 7 pb mainly including $D^*\bar{D}^*$ with a cross section of $\sim$ 5 nb, $D^*\bar{D} + D\bar{D}^*$ with a cross section of $\sim$ 2 nb, and $D\bar{D}$ with a cross section of relatively small $\sim$ 0.2 nb. There also appears to be $D\bar{D}^*\pi$ production. The underlying light quark "continuum" background is about 12 nb. The relatively large cross sections, relatively large branching fractions, and sufficient luminosities allow us to employ double tag (DT) technique to study the semileptonic decay, which was first applied by the Mark III Collaboration [21] in study of semileptonic decays. In this paper we designate D_s^- as the tag, and examine the semileptonic decay of the D_s^+, though in reality we use both charges for tags and signals. The inclusion of charge conjugate reactions is always implied throughout this document.

Since most of D_s events are formed in the process of $e^+e^- \to D_s^* D_s, D_s^* \to \gamma D_s$, we only reconstruct this kind of process. As shown in Fig. 2, D_s^- meson is reconstructed as single tag (ST), then the signal process of $D_s^+ \to K^+K^-e^+\nu_e$ is searched at the recoiling side. This allows us to define a tag sample in which a D_s^- is reconstructed in a hadronic decay mode. Then, in addition to the tag, we define a sub-sample involving a positron and a set of hadrons as a signature of a semileptonic decay.

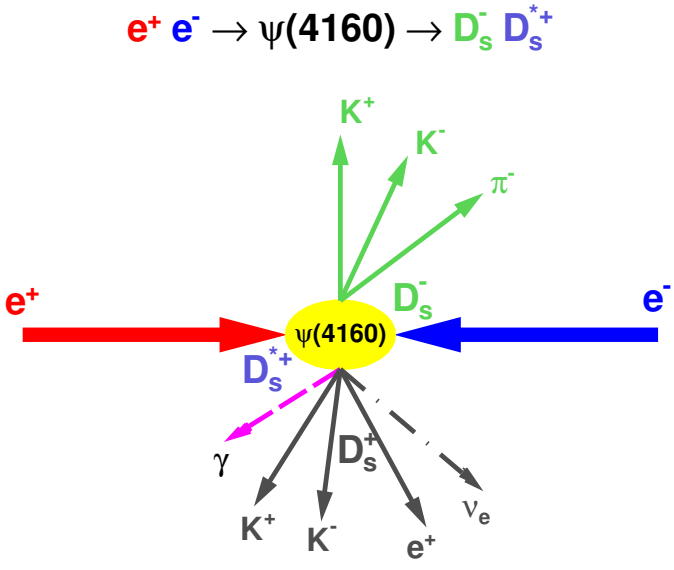

Figure 2: Topology plot of a typical event of $D_s^+ \to K^+K^-e^+\nu_e$

To measure the branching fraction of semileptonic decay, we start from the following equations with one tag mode:

$$N_{tag}^{obs} = 2N_{D_s^* D_s}\mathcal{B}_{tag}\epsilon_{tag}, \tag{1}$$

$$N_{sig}^{obs} = 2N_{D_s^* D_s}\mathcal{B}_{tag}\mathcal{B}_{sig}\mathcal{B}_{\gamma}\epsilon_{tag,sig}, \tag{2}$$

where $N_{D_s^* D_s}$ is the total number of $D_s^{*\pm} D_s^{\mp}$ produced from e^+e^- collision; N_{tag}^{obs} is the number of observed tag modes; N_{sig}^{obs} is the number of observed semileptonic decays (reconstructed with a tag); $\mathcal{B}_{tag}$ is the branching fraction of specific tag mode; $\mathcal{B}_{sig}$ is the branching fraction of the semileptonic decay; $\mathcal{B}_{\gamma}$ is the branching fraction of $D_s^* \to \gamma D_s$; ϵ_{tag} is the reconstruction efficiency of the tag mode; $\epsilon_{tag,sig}$ is the reconstruction efficiency of both the tag and semileptonic decay modes. Using the above two equations it is easy to obtain the following formula:

$$\mathcal{B}_{sig} = \frac{N_{sig}^{obs}\epsilon_{tag}}{\mathcal{B}_{\gamma} N_{tag}^{obs}\epsilon_{tag,sig}}, \tag{3}$$

where the yields N_{tag}^{obs} and N_{sig}^{obs} can be obtained from data, while ϵ_{tag} and $\epsilon_{tag,sig}$ can be obtained from the appropriate Monte-Carlo (MC) samples. The above equations can be generalized to more tag modes in this analysis as follows:

$$\mathcal{B}_{sig} = \frac{N_{sig}^{obs}}{\mathcal{B}_{\gamma} \sum_{\alpha} N_{tag}^{\alpha}\epsilon_{tag,sig}^{\alpha}/\epsilon_{tag}^{\alpha}}, \tag{4}$$

where α = 1, 2, 3, ... represents the tag mode, N_{tag}^{α} is the number of observed tag mode α, N_{sig}^{obs} is the total signal yield with all tag modes. This analytic strategy is usually called as DT method.

3 The BESIII Detector and the Data Samples

3.1 The BESIII Detector

The BESIII detector is a magnetic spectrometer [22] located at the Beijing Electron Positron Collider (BEPCII) [23]. The cylindrical core of the BESIII detector consists of a helium-based multilayer drift chamber (MDC), a plastic scintillator time-of-flight system (TOF), and a CsI(Tl) electromagnetic calorimeter (EMC), which are all enclosed in a superconducting solenoidal magnet providing a 1.0 T magnetic field. The solenoid is supported by an octagonal flux-return yoke with resistive plate counter muon identifier modules interleaved with steel. The acceptance of charged particles and photons is 93% over 4π solid angle. The charged-particle momentum resolution at 1 GeV/c is 0.5%, and the dE/dx resolution is 6% for the electrons from Bhabha scattering. The EMC measures photon energies with a resolution of 2.5% (5%) at 1 GeV in the barrel (end cap) region. The time resolution of the TOF barrel part is 68 ps, while that of the end cap part is 110 ps. The end cap TOF system is upgraded in 2015 with multi-gap resistive plate chamber technology, providing a time resolution of 60 ps [24].

3.2 Data and Monte Carlo Samples

This analysis is performed under BESIII offline software system (BOSS) with version BOSS 7.0.3. So, we use the following data sets and Monte Carlo (MC) samples which are reconstructed with this software environment.

Data:

An integrated luminosity of 3.19 fb^{-1}data set [25] taken at E_{cm} = 4.178 GeV in 2016 with the BESIII detector is used in this analysis, which is reconstructed at BOSS 7.0.3.

Generic MC:

To determine single tag efficiencies, estimate backgrounds (Bkg) and optimize selection criteria, we study the Generic MC samples. They are produced with the Geant4-based [26] MC package which includes the geometric description of the BESIII detector and the detector response. The simulation includes the beam energy spread and initial state radiation (ISR) in the e^+e^- annihilations modelled with the generator KKMC [27] and conExc [28]. The signal and open charm processes are generated with conExc model. The known decay modes are modelled with BesEvtGen [29] developed from EvtGen [30] using branching fractions taken from the Particle Data Group (PDG) [20], and the remaining unknown decays from the charmonium states with LundCharm [31]. The final state radiations (FSR) from charged final state particles are incorporated with the Photos package [32].

These samples are generated and reconstructed under BOSS 7.0.3 by the charm group. There are 40 sets of Generic MC samples (round01~round40), and each of them is equivalent to our data set. The

detail of the components is shown in Table 2. For more information, please refer to the official charm website: http://docbes3.ihep.ac.cn/ charmgroup/index.php/MC_Samples.

Table 2: Generic MC samples. In the column "Generator: event number ≈ times of data".

Physics process	Cross section (nb)	Generator: event number ($\times 10^6$) ≈ times of data
$D^0\bar{D}^0$	0.179	BesEvtGen+conExc: 23 ≈ 40×
D^+D^-	0.197	BesEvtGen+conExc: 25 ≈ 40×
$D^0\bar{D}^{*0} + \bar{D}^0D^{*0}$	1.211	BesEvtGen+conExc: 155 ≈ 40×
$D^+D^{*-} + D^-D^{*+}$	1.296	BesEvtGen+conExc: 166 ≈ 40×
$D^{*0}\bar{D}^{*0}$	2.173	BesEvtGen+conExc: 278 ≈ 40×
$D^{*+}D^{*-}$	2.145	BesEvtGen+conExc: 274 ≈ 40×
$D_s^+D_s^-$	0.007	BesEvtGen+conExc: 0.9 ≈ 40×
$D_s^{*+}D_s^- + D_s^{*-}D_s^+$	0.889	BesEvtGen+conExc: 123 ≈ 40×
$D\bar{D}^*\pi^\pm + \bar{D}D^*\pi^\pm$	0.383	BesEvtGen+conExc: 49 ≈ 40×
$D\bar{D}^*\pi^0 + \bar{D}D^*\pi^0$	0.192	BesEvtGen+conExc: 25 ≈ 40×
$D\bar{D}\pi^\pm$	0.050	BesEvtGen+conExc: 6 ≈ 40×
$D\bar{D}\pi^0$	0.025	BesEvtGen+conExc: 3 ≈ 40×
$e^+e^- \to q\bar{q}$ (u, d, s)	13.8	KKMC: 1764 ≈ 40×
$e^+e^- \to \gamma_{ISR}J/\psi$	0.40	BesEvtGen: 51 ≈ 40×
$e^+e^- \to \gamma_{ISR}\psi(3686)$	0.42	BesEvtGen: 54 ≈ 40×
$e^+e^- \to \gamma_{ISR}\psi(3770)$	0.06	BesEvtGen: 8 ≈ 40×
$e^+e^- \to \tau^+\tau^-$	3.45	KKMC: 441 ≈ 40×
$e^+e^- \to \mu^+\mu^-$	5.24	Babayaga [33]: 670 ≈ 35×
$e^+e^- \to e^+e^-$	423.99	Babayaga: 542 ≈ 0.01×
two photon fusion	1.7	BesTwogam [29]: 217 ≈ 40×
$\pi\pi(\psi(2S)/h_c/J/\psi), (KK/\eta)J/\psi$	0.1	BesEvtGen+conExc: 13 ≈ 40×

Exclusive MC:

The following exclusive MC samples are generated at BOSS 7.0.3 using BesEvtGen generator. For them, we employ conExc model to generate the final state of $D_s^*D_s$ where D_s^* only decays to γD_s.

- **Signal MC**

  A: 4M sample of $D_s^- \to anything$, $D_s^+ \to \phi e^+\nu_e$, $\phi \to K^+K^-$, where D_s^- decays generically and D_s^+ decays to $\phi e^+\nu_e$, $\phi \to K^+K^-$ according to the nominal PWA solution where only P-wave component ϕ is considered and the other components are set to zero. This sample is used to model the MM^2 distribution of the signal and obtain the signal efficiency.

  B: 4M sample of $D_s^- \to anything$, $D_s^+ \to \phi e^+\nu_e$, $\phi \to K^+K^-$, where D_s^- decays generically and D_s^+ decays to $\phi e^+\nu_e$, $\phi \to K^+K^-$ using the default generator (ISGW2) in BesEvtGen package. This sample is used to make input-output check for the branching fraction measurement.

- **Bkg MC**

  4M sample of $D_s^- \to anything$, $D_s^+ \to f_0(980)e^+\nu_e$, $f_0(980) \to K^+K^-$, where D_s^- decays generically and $f_0(980)$ is parameterized by the Flatté formula with its parameters g_1, g_2 fixed to the BESII

measurements [34] and the mass mean fixed to a new BESIII measurement [35]. This sample is used for the DT efficiency to estimate the yield of this peaking background and the shape of the MM^2 distribution.

- **DIY MC**

  40M sample of $D_s^- \to tags$, $D_s^+ \to \phi e^+ \nu_e$, $\phi \to K^+K^-$, where D_s^- decays to tag modes and D_s^+ decays to $\phi e^+ \nu_e$, $\phi \to K^+K^-$, according to the nominal PWA solution where only P-wave component ϕ is considered and the other components are set to zero. This sample is used to calculate the MC integration in finding the final PWA solution and make fitting procedure checks.

4 Event Selection and Analysis Techniques

The single tags are reconstructed in the channels with large branching fractions and low background levels. After the reconstruction of the single tags, the signal decay $D_s^+ \to K^+K^-e^+\nu_e$ could be selected. The particle identification (PID) and selection criteria are essentially the same for the tracks from both single tag and signal side. We describe the details of these selection criteria in the following.

4.1 Particle Identification and Selection

4.1.1 Charged Track Selection

Charged tracks reconstructed by MDC hit information must be fitted by Kalman method successfully and come from the interaction region in three dimensions. Due to changing beam conditions, the interaction point (IP) moves. Thus, a separate average IP (beam position) is determined for each run using the **VertexDbSvc** package. Relative to this run-dependent IP, each charged track must satisfy the following requirements:

- the polar angle: $|cos\theta| < 0.93$,
- distance of the track from the beam position in x-y plane: $|dr| < 1$ cm,
- distance of the track from the beam position in z plane: $|dz| < 10$ cm.

4.1.2 Neutral Track Selection

Showers are mainly used in π^0 reconstruction, and they must satisfy fiducial and shower-quality requirements as the following:

- minimum energy requirement for barrel showers ($|cos\theta| < 0.8$): $E_{min} > 25$ MeV,
- minimum energy requirement for end-cap showers ($0.86 < |cos\theta| < 0.92$): $E_{min} > 50$ MeV,
- EMC time requirement in this analysis (there are more than one charged track reconstructed): $0 \le T \le 14$ (unit: 50ns).

4.1.3 K, π and e Selection

K, π and e are identified with tracks which satisfy good charged track requirements described in Sec. 4.1.1 using **ParticleID** package (ParticleID-00-04-62), which utilizes both dE/dx and TOF information. By combining dE/dx and TOF χ variables with $\chi^2 = \chi^2_{dE/dx} + \chi^2_{TOF}$ and the corresponding number of freedoms, the probabilities of K/π hypotheses for every charged track are obtained. For K/π identification, we require:

K: $Prob(K) > Prob(\pi)$ and $Prob(K) > 0$,

π: $Prob(\pi) > Prob(K)$ and $Prob(\pi) > 0$.

For e identification, in addition to dE/dx and TOF information, EMC measurements are also used. Similar to K/π PID, the probabilities of $K/\pi/e$ hypotheses are calculated and we require:

$Prob(e)/(Prob(e) + Prob(\pi) + Prob(K)) > 0.8$ and $0.8 < E/p < 1.2$,

where E is the depositional energy of e in EMC and p is the momentum reconstructed in MDC. Since the ratio between them is close to 1, we require the above region requirement.

4.1.4 π^0 and η Selection

π^0 and η are reconstructed with a pair of photons which satisfy requirements described in Sec. 4.1.2. To reduce the background from false photons, additionally, we require that the cluster position of the photon is more than 20° from calorimeter entrance of any track. Candidates with both photons from end-cap EMC regions are rejected because of the bad resolution. An unconstrained mass $M(\gamma\gamma)$ is calculated from energies and momenta of the two photon pairs. A kinematic fit of the two photons to the π^0/η mass [20] is also performed and the resulting energies and momentum of the π^0/η is saved for further analyses. Then π^0 or η candidates are required to satisfy the following requirements:

- χ^2 value from kinematic fit: $\chi^2 < 30$,
- the unconstrained mass of π^0 : $0.115\ \text{GeV}/c^2 < M(\gamma\gamma) < 0.150\ \text{GeV}/c^2$.
- the unconstrained mass of η: $0.49\ \text{GeV}/c^2 < M(\gamma\gamma) < 0.58\ \text{GeV}/c^2$.

4.1.5 K_S^0 Selection

K_S^0 candidates are reconstructed using `VeeVertexAlg` package with two oppositely charged tracks. The charged tracks are not subject to good track requirements described in Sec. 4.1.1 and PID. The requirements on the daughter tracks are:

- the polar angle: $|cos\theta| < 0.93$,
- distance of the track from the beam position in z plane: $|dz| < 20$ cm.

For each pair of tracks, a constrained vertex fit is performed and the resulting track parameters are used to get invariant mass $M(\pi\pi)$. The requirements for K_S^0 candidate are as follows:

- χ^2 value from the vertex fit: $\chi^2 < 100$,
- mass window: $0.487\ \text{GeV}/c^2 < M_{\pi\pi} < 0.511\text{GeV}/c^2$.

4.1.6 ρ Selection

The ρ^0 and ρ^- mesons are reconstructed with $\pi^+\pi^-$ and $\pi^-\pi^0$ combinations. For ρ^0, we require the $\pi^+\pi^-$ invariant mass within the range: $0.570\ \mathrm{GeV}/c^2 < M_{\pi^+\pi^-} < 0.970\ \mathrm{GeV}/c^2$. For ρ^-, we require the $\pi^-\pi^0$ invariant mass within the range: $|M_{\pi^-\pi^0} - M_{\rho^-}| < 0.150\ \mathrm{GeV}/c^2$, where M_{ρ^-} is used from PDG [20].

4.1.7 η' Selection

The η' candidates are reconstructed by the decay of $\eta' \to \pi^+\pi^-\eta$ and $\eta' \to \gamma\rho^0$, respectively. They are required to satisfy:

- $0.943\ \mathrm{GeV}/c^2 < M_{\pi^+\pi^-\eta} < 0.973\ \mathrm{GeV}/c^2$.
- $0.938\ \mathrm{GeV}/c^2 < M_{\gamma\rho^0} < 0.978\ \mathrm{GeV}/c^2$, and $E_\gamma > 100$ MeV.

4.1.8 Other Specific Selections

In order to suppress the backgrounds from D^* decay, we require that the minimum momentum of all pions is greater than 100 MeV/c. For the detail, please see the previous D_s study [36].

Since we use both of tag modes $D_s^- \to K_S^0 K^-$ and $D_s^- \to K^-\pi^+\pi^-$, we require the $\pi^+\pi^-$ invariant mass from $D_s^- \to K^-\pi^+\pi^-$ outside of the range: $0.475\ \mathrm{GeV}/c^2 < M_{\pi^+\pi^-} < 0.520\ \mathrm{GeV}/c^2$ to exclude the pollution of K_S^0 from the process $D_s^- \to K_S^0 K^-$.

4.2 Single Tag Candidate Selection

The D_s^- candidates are reconstructed by looping all these daughter tracks to form different combinations. The final state of D_s^- meson includes charged K/π, neutral π^0, $\eta^{(\prime)}$ and K_S^0 which satisfy the previous particle selection. D_s^- meson reconstruction is performed with **DTagAlg** package (DTagAlg-00-01-05) using default settings as described in Sec. 4.1 . We use the following decay channels as single tag modes: $D_s^- \to K^+K^-\pi^-$, $D_s^- \to K_S^0K^-$, $D_s^- \to \pi^-\eta$, $D_s^- \to \pi^-\eta'_{\pi^+\pi^-\eta}$, $D_s^- \to K^+K^-\pi^-\pi^0$, $D_s^- \to \pi^+\pi^-\pi^-$, $D_s^- \to K_S^0K^+\pi^-\pi^-$, $D_s^- \to \rho^-_{\pi^-\pi^0}\eta$, $D_s^- \to \pi^-\eta'_{\gamma\rho^0}$, $D_s^- \to K^+\pi^-\pi^-$, $D_s^- \to K_S^0K^-\pi^0$, and $D_s^- \to K_S^0K^-\pi^+\pi^-$.

In order to identify the process $e^+e^- \to D_s^*D_s$, we define the recoil mass of the single tag candidate $\mathrm{M_{rec}}$ as below:

$$\mathrm{M_{rec}} = \sqrt{(E_{cm} - \sqrt{|\boldsymbol{p}_{D_s}|^2 + m_{D_s}^2})^2 - |\boldsymbol{p}_{cm} - \boldsymbol{p}_{D_s}|^2}, \tag{5}$$

where $(E_{cm}, \boldsymbol{p}_{cm})$ is the e^+e^- center of mass four-vector, $\boldsymbol{p}_{D_s}$ is the measured D_s momentum with calibration, and M_{D_s} is the nominal D_s mass [20]. As shown in Fig. 3, for indirect D_s candidates who are the daughter of a D_s^*, $\mathrm{M_{rec}}$ peaks at the D_s^* mass of $2.112\ \mathrm{GeV}/c^2$; for direct D_s candidates produced in the

initial $e^+e^- \to D_s^* D_s$ process, M_{rec} spreads roughly ± 65 MeV/c^2 around this peak. In order to suppress the backgrouds, we require M_{rec} to satisfy: $2.05 < M_{rec} < 2.18$ GeV/c^2; this accepts all kinematically allowed events and removes the $D_s^+ D_s^-$ events that peak at $M_{rec} = D_s$ mass. If there are multiple candidates per mode and charge, we chose the one with M_{rec} closest to D_s^* mass [20].

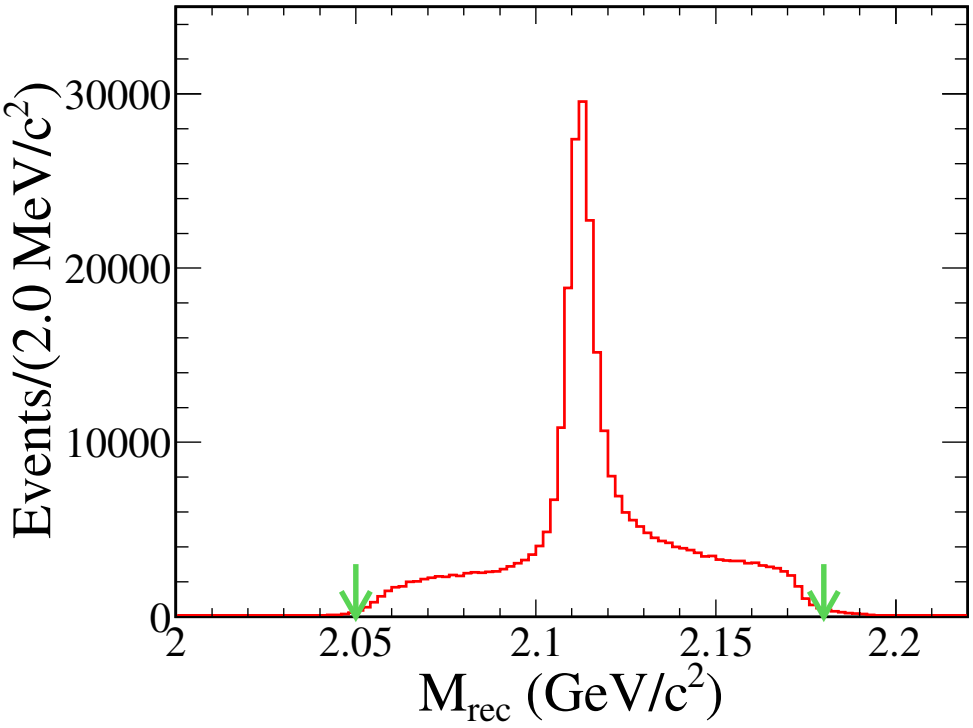

Figure 3: M_{rec} distribution from $D_s^* D_s$ MC. We make truth match for them, and the green arrows denote the signal region.

The yields for each tag mode are obtained by fitting the D_s Mass distribution of the events passing the previous selection criterion. The fitting function is a sum of the signal and the background shape. The description of the signal is based on the reconstructed MC shape convoluted with a Gaussian function. The MC shape is required to match the truth information [37]. The Gaussian resolution and the mean are free parameters in the fit, thus allowing to correct for possible biases on the resolution and the peak position in the simulation. The background is described by a first-order Chebyshev polynomial function. The fits to the D_s Mass distributions of data are shown in Fig. 4. The tag yield of data and D_s Mass window for each mode are summarized in Table 3. Then, we obtain the total 380305 ± 2314 reconstructed tags. After single tag reconstruction, we search the signal of D_s semileptonic decay within the D_s mass selection region.

Single tag efficiencies are obtained with 40 round Generic MC samples by calculating the ratio of a MC yield and a MC truth total. The tag yields of MC for each round are obtained with exactly the same

method as data yield, which can minimize systematics. The denominators are obtained from counting events in the MC truth information at the generator level. For the MC truth counting, the detail can be found in the memo [37]. The total reconstruted tag yields and single tag efficiency for each tag modes are listed in Table 4.

Table 3: D_s Mass window, single tag yields, background yields, χ^2/ndf value and fractions of all tags for data in each tag mode.

D_s Tag Mode	Mass region GeV/c^2	N_{tag}^{obs}	Bkg Yields	χ^2/ndf	Fractions(%)
$D_s^- \to K^+K^-\pi^-$	1.950 ~ 1.986	135141 ± 616	180589±436	1.24	35.50
$D_s^- \to K_S^0K^-$	1.948 ~ 1.991	32539 ± 315	23965±191	1.18	8.56
$D_s^- \to \pi^-\eta$	1.930 ~ 2.000	18705 ± 734	68787±724	0.95	4.92
$D_s^- \to \pi^-\eta'_{\pi^+\pi^-\eta}$	1.938 ~ 1.997	8310 ± 155	7509±133	1.16	2.19
$D_s^- \to K^+K^-\pi^-\pi^0$	1.940 ~ 1.987	39835 ± 851	255204±761	0.96	10.47
$D_s^- \to \pi^+\pi^-\pi^-$	1.950 ~ 1.987	38725 ± 934	404565±750	0.94	10.18
$D_s^- \to K_S^0K^+\pi^-\pi^-$	1.947 ~ 1.990	16070 ± 298	72081±287	1.08	4.23
$D_s^- \to \rho^-_{\pi^-\pi^0}\eta$	1.920 ~ 2.000	30307 ± 1096	216721±1162	1.14	7.97
$D_s^- \to \pi^-\eta'_{\gamma\rho^0}$	1.935 ~ 1.990	23470 ± 757	186665±720	0.80	6.17
$D_s^- \to K^-\pi^+\pi^-$	1.953 ~ 1.983	16760 ± 749	271593±541	1.04	4.41
$D_s^- \to K_S^0K^-\pi^0$	1.935 ~ 1.990	12331 ± 469	121212±492	1.26	3.24
$D_s^- \to K_S^0K^-\pi^+\pi^-$	1.955 ~ 1.982	8112 ± 271	83806±228	1.03	2.13

Table 4: The Generated events number, reconstructed tag yields and single tag efficiency for 40 round Generic MC in each tag mode. In some tag modes, $K_S^0 \to \pi^+\pi^-$ and $\eta/\pi^0 \to \gamma\gamma$ are required.

D_sTag Mode	Generated	Reconstructed	$\epsilon_{tag}(\%)$
$D_s^- \to K^+K^-\pi^-$	13407817	5417137 ± 3361	40.40 ± 0.025
$D_s^- \to K_S^0K^-$	2599655	1290250 ± 1576	49.63 ± 0.061
$D_s^- \to \pi^-\eta$	1641259	742296 ± 2422	45.23 ± 0.148
$D_s^- \to \pi^-\eta'_{\pi^+\pi^-\eta}$	1633571	342144 ± 937	20.94 ± 0.057
$D_s^- \to K^+K^-\pi^-\pi^0$	14620284	1605542 ± 4124	10.98 ± 0.028
$D_s^- \to \pi^+\pi^-\pi^-$	2937301	1529981 ± 3913	52.09 ± 0.133
$D_s^- \to K_S^0K^+\pi^-\pi^-$	2846013	653934 ± 1565	22.98 ± 0.055
$D_s^- \to \rho^-_{\pi^-\pi^0}\eta$	8746776	1378776 ± 5717	15.76 ± 0.065
$D_s^- \to \pi^-\eta'_{\gamma\rho^0}$	2776998	850031 ± 3547	30.61 ± 0.128
$D_s^- \to K^-\pi^+\pi^-$	1417408	642434 ± 3278	45.32 ± 0.231
$D_s^- \to K_S^0K^-\pi^0$	2618290	487980 ± 2991	18.64 ± 0.114
$D_s^- \to K_S^0K^-\pi^+\pi^-$	1626325	322664 ± 1734	19.84 ± 0.107

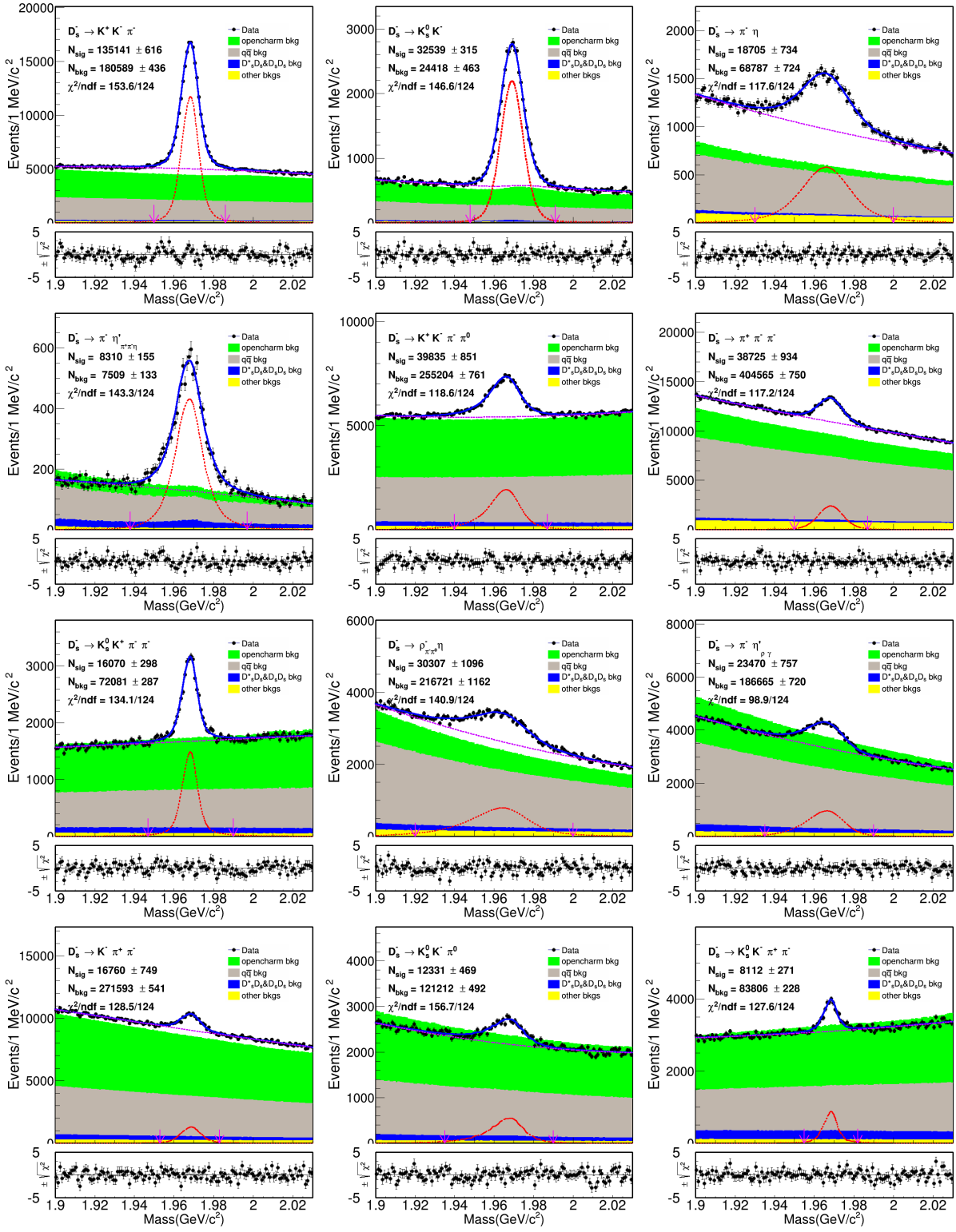

Figure 4: D_s Mass fits from data. The points with error bars are data, and the blue line is the fit. Red short-dashed lines are signal, violet long-dashed lines are background. The red arrows denote the signal region.

4.3 Signal Candidate Selection

After a tag is identified, we search for the $D_s^+ \to K^+K^-e^+\nu_e$ process recoiling against the tag side, requiring exactly three good charged tracks identified as K^+, K^- and e^+ (opposite sign to the D_s^- tag). Since most of D_s^* decay to γDs final state, we reconstruct this transition photon and require one more good photon candidate. For the particles from semileptonic decay side and the photon candidate (s), their identification and reconstruction are the same with tag side as in Sec. 4.1. These tracks which are not used in the tag side are selected to make up the final candidate. The combined tag and semileptonic decay candidate must account for all tracks in the event and satisfy charge conservation.

Since the neutrino is undetectable, we only need to find the transition photon if there are multiple photon candidates. To select the best photon candidate, a kinematic fit is performed to each event based on two hypotheses, one of which is that the D_s^- tag is the daughter of a D_s^{*-}, and the other that the semileptonic decay D_s^+ is the daughter of a D_s^{*+}. Thus, we constrain the total four-momentum to the e^+e^- center-of-mass frame, the invariant mass of the D_s^- tag, the D_s^+ signal and the D_s^* to their known mass [20]. This gives us a total of seven constraints (7C). The missing nenutrino four-vector needs to be determined, so we are left with a three-constraint fit (3C). After an iterative fit with two hypotheses, we choose the photon and the decay sequence in each event with the minimum χ^2_{3C}.

Regardless of whether or not the photon forms a D_s^* with the tag, for real $D_s^*D_s$ events, the recoiling mass squared $\mathrm{M}^2_{\mathrm{rec}}$ against the photon and the D_s^- tag should peak at the D_s mass-squared. We calculate it as below:

$$\mathrm{M}^2_{\mathrm{rec}} = (E_{cm} - E_{D_s} - E_\gamma)^2 - (\boldsymbol{p}_{cm} - \boldsymbol{p}_{D_s} - \boldsymbol{p}_\gamma)^2, \tag{6}$$

where E_{cm} ($\boldsymbol{p}_{cm}$) is the center-of-mass energy (momentum), E_{D_s} ($\boldsymbol{p}_{D_s}$) is the energy (momentum) of the fully reconstructed D_s^- tag, and E_γ ($\boldsymbol{p}_\gamma$) is the energy (momentum) of the selected photon. To improve the resolution, we constrain the decay products of the D_s^- tag to the known D_s mass [20]. To suppress the background and have higher signal efficiency, we require $\mathrm{M}^2_{\mathrm{rec}}$ to satisfy 3.78 GeV$^2/c^4$< $\mathrm{M}^2_{\mathrm{rec}}$ < 4.05 GeV$^2/c^4$. We also give the comparisons between data and MC as shown in Fig. 5.

To guarantee the event from ϕ signal region, we require Mass($\mathrm{K^+K^-}$) to satisfy 1.005 GeV/c^2< Mass($\mathrm{K^+K^-}$) < 1.05 GeV/c^2. The low-end requirement that is about 3σ off the mean of ϕ is used to reduce the possible events from the $f_0(980)$ while the high-end requirement is used to retain the high-end mass tail. In the Mass($\mathrm{K^+K^-}$) distribution with log scale set, we find that there is obvious difference between data and MC due to the process $f_0(980) \to K^+K^-$. By checking the Generic MC generation, we find the $f_0(980)$ is generated using simple Breit-Wiger shape with 990 MeV/c^2 mass and 50 MeV/c^2 width which lead to much higher efficiency. In the following background analysis (Sec 4.4), we describe the treatment for this process. The comparisons of data and MC are shown in Fig. 6.

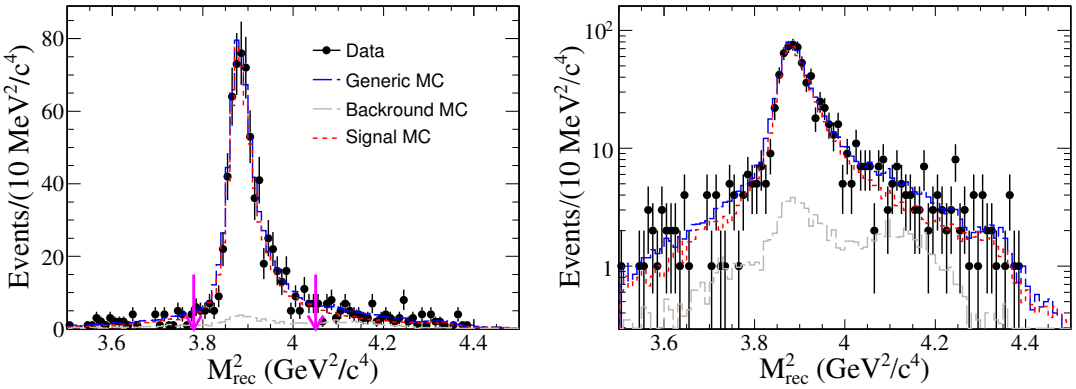

Figure 5: M^2_{rec} distributions of data and MC (Rigt plot in log scale). The red arrows denote the signal region that we require. The points with error bars are data, and the blue long-dashed lines are Generic MC. The red short-dashed lines are signal MC and the gray long-dashed lines are backgrounds from Generic MC.

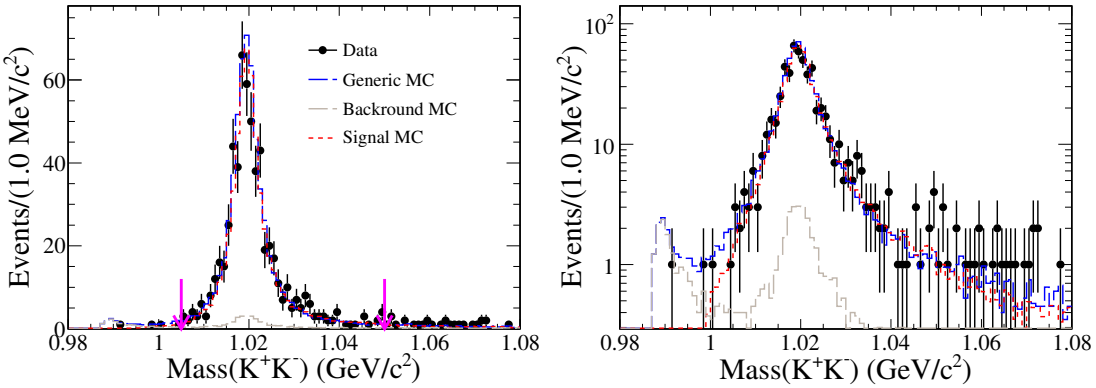

Figure 6: Mass(K^+K^-) distributions of data and MC (Rigt plot in log scale). The red arrows denote the signal region that we require. The points with error bars are data, and the blue long-dashed lines are Generic MC. The red short-dashed lines are signal MC and the gray long-dashed lines are backgrounds from Generic MC.

Finally, we define a variable of the missing mass squared MM^2 to reconstruct the missing neutrino, by which the semileptonic decay is identified. The MM^2 is defined as below:

$$\mathrm{MM}^2 = (E_{cm} - E_{D_s} - E_{K^+} - E_{K^-} - E_e - E_\gamma)^2 - (\boldsymbol{p}_{cm} - \boldsymbol{p}_{D_s} - \boldsymbol{p}_{K^+} - \boldsymbol{p}_{K^-} - \boldsymbol{p}_e - \boldsymbol{p}_\gamma)^2, \tag{7}$$

where E_e ($\boldsymbol{p}_e$) is the center-of-mass energy (momentum) of the candidate positron, E_K ($\boldsymbol{p}_K$) is the energy (momentum) of the candidate kaon, and all the other variables are the same as defined in Eq. 6. To improve the resolution, we correct the momentum of the D_s^- tag and γ based on 3C kinematic fit method. After satisfying all the above requirements, we obtain the MM^2 distribution as shown in Fig. 7. By studying the Generic MC, we find that the backgrounds level for the process $D_s^+ \to \phi e^+ \nu_e$, $\phi \to K^+K^-$ is about 8.0%, and the main components are peaking backgrounds. The events in the tag D_s Mass sideband regions from data also shows that there are peaking backgrounds. The sideband regions having the same interval as the tag D_s region are symmetrically located on both sides of the tag D_s mass peaking and 2σ away from the tag region.

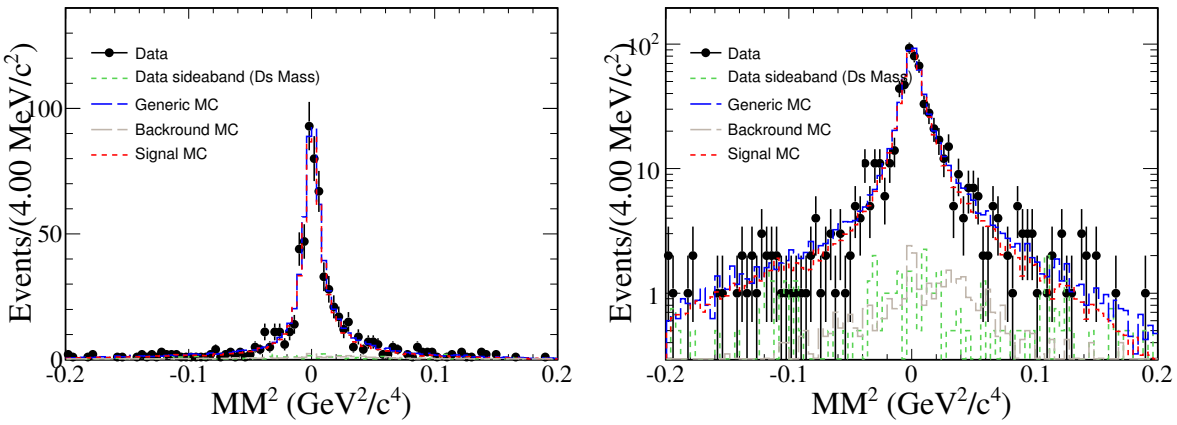

Figure 7: MM^2 distributions of data and MC (Rigt plot in log scale). The points with error bars are data, and the blue long-dashed lines are Generic MC. The red short-dashed lines are signal MC; the gray long-dashed lines are backgrounds from Generic MC; the green short-dashed lines are from data sideband using tag D_s Mass.

4.4 Background Analysis

For the process $D_s^+ \to \phi e^+ \nu_e$, $\phi \to K^+K^-$, we study the background components with Generic Monte Carlo samples as shown in Table 2. These backgrounds satisfying the selection criteria must be subtracted and their number can be estimated by analyzing the Generic MC sample. As shown in Table. 5, the most of the background events are from $D_s^* D_s$ process, and the second backgrounds are from $q\bar{q}$ process and other open charm processes.

For the backgrounds of $D_s^* D_s$ process, almost half of them (48.9%) are the $D_s^{*+} \to D_s^+ \pi^0$ decay where D_s^+ mostly decay to our signal process and the rest are the wrong combinations from $D_s^{*+} \to D_s^+ \gamma$ decay, where in most situation at least one D_s decay to a hadronic mode (tipically $K^+K^-\pi^\pm$ and $\phi\rho^\pm$) including K^+K^- final state or a semileptonic decay mode ($\phi(K^+K^-)\mu\nu_\mu$, $\eta(\gamma\gamma)e\nu_e$, $\eta'(\pi^+\pi^-\gamma)e\nu_e$ and $f_0(980)(\pi^+\pi^-)e\nu_e$). As shown in Fig. 8, all of them have been scaled to data size. The background level is about 8.0% based on Generic MC study.

The peaking background from $D_s^+ \to f_0(980)e^+\nu_e, f_0(980) \to K^+K^-$ is still 11.6% of the total background MC even with the low-end requirement based on the current MC simulation. Furthermore, we indeed find the obvious difference between data and MC by checking the Mass(K^+K^-) distribution at low-end. So, the shape and yield of this peaking background needs to be re-estimated. For the shape, we parametrize the $f_0(980)$ by the Flatté formula, which is described as Bkg MC sample in Sec. 3.2. For the yield, we firstly obtain the new branching fraction of $D_s^+ \to f_0(980)e^+\nu_e, f_0(980) \to K^+K^-$ using the new measurement [35]: $\mathcal{B}(D_s^+ \to f_0(980)e^+\nu_e, f_0(980) \to \pi^+\pi^-) = (1.67 \pm 0.18 \pm 0.07) \times 10^{-3}$ and the ratio $\frac{\mathcal{B}(f_0(980)\to K^+K^-)}{\mathcal{B}(f_0(980)\to\pi^+\pi^-)} = 0.35^{+0.15}_{-0.14}$ averaged with the previous measurements from BES [38] and BABAR [39]. Then, by a simple derivation of the Eq. 4 where the DT efficiencies are obtained from the Bkg MC sample, a new yield of this peaking background could be calculated to be $N_{f_0(980)\to K^+K^-} = 12.2^{+5.4}_{-5.1}$. In the following branching fraction and form factor measurement for $D_s^+ \to \phi e^+\nu_e$, we use this new generated Bkg MC sample to substitute the old MC for this peaking process.

Table 5: The different background yields and fractions from 40 rounds of Generic MC.

Souce	MC Bkg Yields	Fraction (%)
$D_s^* D_s$	46.85	83.25
Other open charm	4.10	7.28
$q\bar{q}$	5.20	9.24
Others	0.13	0.22

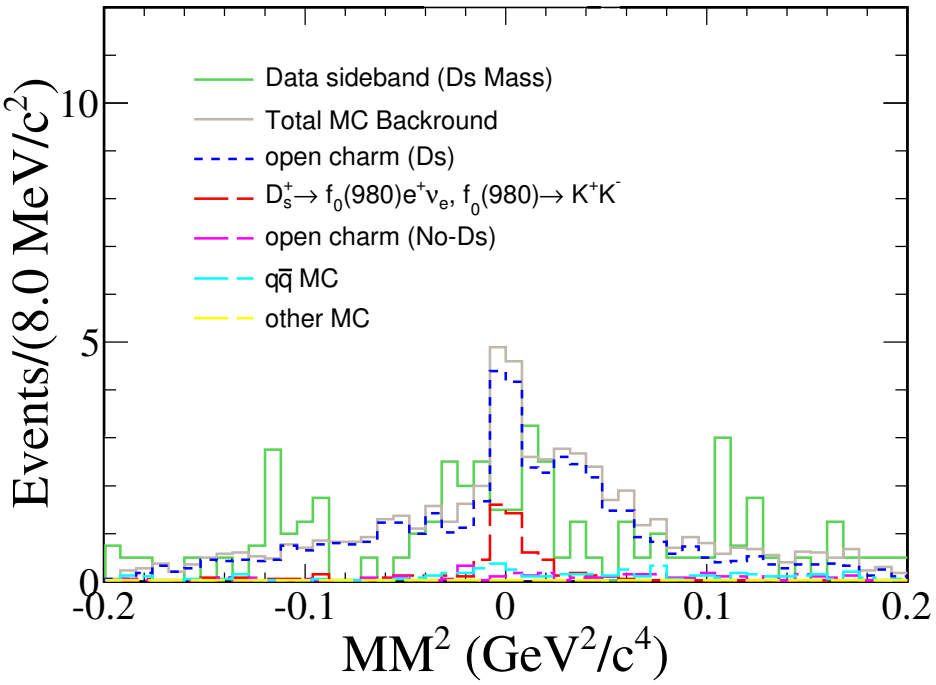

Figure 8: MM^2 distribution from MC events and data sideband (Mass), where all of them are scaled to data size. Most of them are from $D_s^* D_s$ process, and the second sources are $q\bar{q}$ process and other open charm processes.

5 Branching Fraction Measurement

5.1 Efficiency of Double Tag Signal

In this work, double-tag signal efficiencies ($\epsilon_{tag,sig}$) are obtained using Signal MC sample A, where the D_s^- meson decays generically on the tag side and the D_s^+ meson decays only through the semileptonic signal channel. After applying the same selection procedure as in the data, the signal yields are obtained by counting to the events of the MM^2 distribution within ± 0.20 GeV^2/c^4. (Here we only need to count events: no fit is required; fake tag plus real signal is also defined as signal and taken into the efficiency). The corresponding signal efficiencies are listed in Table 6.

Table 6: Signal efficiencies of each tag mode for the decay $D_s^+ \to \phi e^+ \nu_e$, $\phi \to K^+K^-$.

Tag Mode	$D_s^+ \to \phi e^+ \nu_e$, $\phi \to K^+K^-$ (%)
$D_s^- \to K^+K^-\pi^-$	5.75 ± 0.05
$D_s^- \to K_S^0K^-$	7.35 ± 0.13
$D_s^- \to \pi^-\eta$	7.37 ± 0.17
$D_s^- \to \pi^-\eta'_{\pi^+\pi^-\eta}$	3.06 ± 0.11
$D_s^- \to K^+K^-\pi^-\pi^0$	1.61 ± 0.03
$D_s^- \to \pi^+\pi^-\pi^-$	7.87 ± 0.13
$D_s^- \to K_S^0K^+\pi^-\pi^-$	3.31 ± 0.08
$D_s^- \to \rho^-_{\pi^-\pi^0}\eta$	2.89 ± 0.05
$D_s^- \to \pi^-\pi'_{\gamma\rho^0}$	4.79 ± 0.10
$D_s^- \to K^-\pi^+\pi^-$	7.25 ± 0.17
$D_s^- \to K_S^0K^-\pi^0$	3.24 ± 0.09
$D_s^- \to K_S^0K^-\pi^+\pi^-$	2.65 ± 0.10

5.2 Double Tag Signal Yields

After applying all the selection criteria, we get total 670 events. By fitting the MM^2 distribution, we could obtain the double tag signal yield. The signal is modeled with signal MC shape smeared with a Gaussian function, and the background is modeled with the generic MC shape, also smeared with the same resolution function. Here the Gaussian function is used to describe the resolution difference between data and MC. The background shape is taken from the generic MC except for the peaking background process $D_s^+ \to f_0(980)e^+\nu_e$, $f_0(980) \to K^+K^-$ which is substituted by our new generated Bkg MC sample as described in Sec. 3.2. The background yield and shape are fixed based on the above new generic MC. As shown in Fig. 9, we obtain 610.2 ± 25.5 signal events. The fit range is from -0.20 GeV^2/c^4 to 0.20 GeV^2/c^4. The efficiency loss of the signal MC events outside of this window is about 2.3% according to the study of Signal MC sample A.

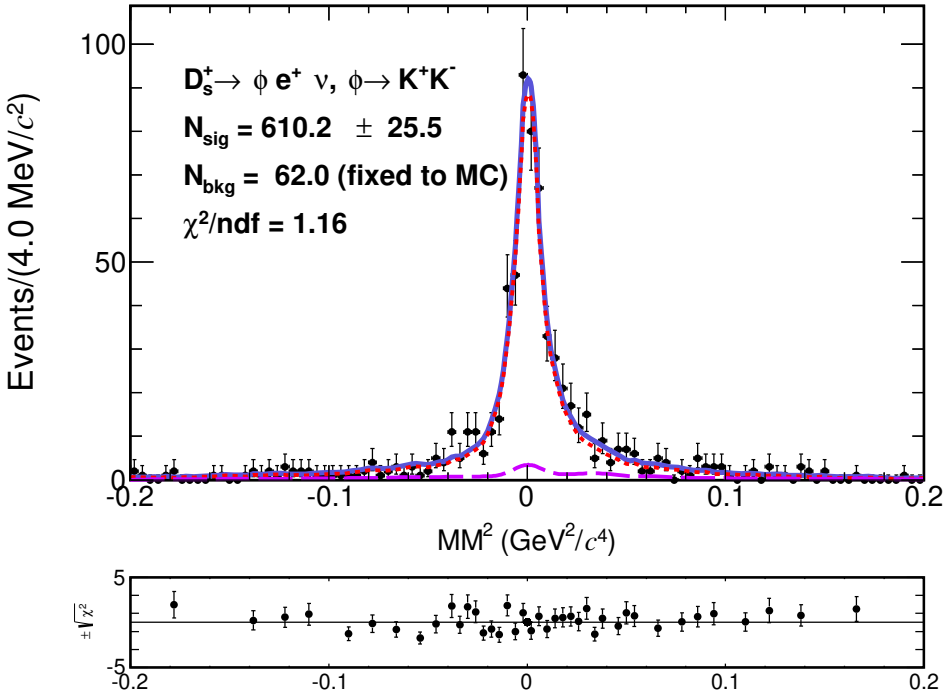

Figure 9: MM^2 fit to data. The points with error bars are data, and the blue line is the fit. The red short-dashed line is signal; the violet long-dashed line is the background from generic MC. For the χ^2/ndf calculation, we merge the neighboring bins with a very few entries till there are 10 entries accumulated.

5.3 Results of Branching Fraction

Using Eq. 4, signal yields in Sec. 5.2 and the efficiencies in Table 6, we can obtain the absolute branching fraction:

$$\mathcal{B}(D_s^+ \to \phi e^+ \nu_e) = \mathcal{B}(D_s^+ \to K^+K^- e^+ \nu_e)/\mathcal{B}(\phi \to K^+K^-) = (2.31 \pm 0.10 \pm 0.09)\%, \tag{8}$$

where the first uncertainties are statistical and the second ones are systematic (described later in this section), $\mathcal{B}(\phi \to K^+K^-) = (49.2 \pm 0.5)\%$ [20]. The branching fraction related to ϕ would lead to 1.0% systematic uncertainty. Our measurement is consistent with the PDG value [20].

5.4 Input and output check

In order to check the validity of analysis method, there are 40 sets of generic MC samples (round:1-40) used for the test, in which the input value of $\mathcal{B}_0(D_s^+ \to \phi e^+ \nu_e)$ is 2.49%. We use the exact same prcoce-dure as for data sample except for the dispose of the peaking background MC from $D_s^+ \to f_0(980)e^+\nu_e$, $f_0(980) \to K^+K^-$. Signal MC sample B is used to get the signal efficiencies where the generator model is same with that used in generic MC samples. We fit each set of generic MC sample to get the tag yield and signal yield, and estimate the tag efficiencies based on the remaining sets of generic MC samples.

In order to estimate the possible bias due to our method, we combine these 40 branching fraction measurements. The estimated mean ($\mu_{\mathcal{B}}$) and its uncertainty σ_μ is calculated with the below formulas:

$$\mu_{\mathcal{B}} = \frac{\sum_i \frac{\mu_i}{\sigma_i^2}}{\sum_i \frac{1}{\sigma_i^2}}, \quad \sigma_\mu^2 = \frac{1}{\sum_i \frac{1}{\sigma_i^2}}, \tag{9}$$

where μ_i and σ_i are the measured branching fraction value and its statistical uncertainty for the sample i. As shown in Table .7, we get 40 sets of measured branching fraction values and the combined result $\mu_{\mathcal{B}} = (2.494 \pm 0.016)\%$. The relative change compared to the input value is only 0.16%, which could be negligible.

Table 7: The absolute branching fraction measurement for round:1 ~ 40.

Round	$\mathcal{B}(D_s^+ \to \phi e^+ \nu_e)(\%)$
1	2.716 ±0.108
2	2.394 ±0.101
3	2.339 ±0.100
4	2.641 ±0.106
5	2.509 ±0.103
6	2.570 ±0.106
7	2.477 ±0.103
8	2.526 ±0.104
9	2.496 ±0.103
10	2.549 ±0.105
11	2.463 ±0.102
12	2.599 ±0.105
13	2.440 ±0.102
14	2.458 ±0.102
15	2.512 ±0.104
16	2.403 ±0.101
17	2.397 ±0.102
18	2.459 ±0.102
19	2.516 ±0.104
20	2.605 ±0.106
21	2.599 ±0.105
22	2.530 ±0.104
23	2.532 ±0.103
24	2.549 ±0.104
25	2.539 ±0.103
26	2.501 ±0.103
27	2.338 ±0.100
28	2.403 ±0.102
29	2.514 ±0.104
30	2.603 ±0.105
31	2.391 ±0.101
32	2.570 ±0.105
33	2.439 ±0.102
34	2.522 ±0.104
35	2.476 ±0.103
36	2.376 ±0.101
37	2.488 ±0.103
38	2.431 ±0.102
39	2.461 ±0.102
40	2.548 ±0.104
Combined result	2.494 ± 0.016

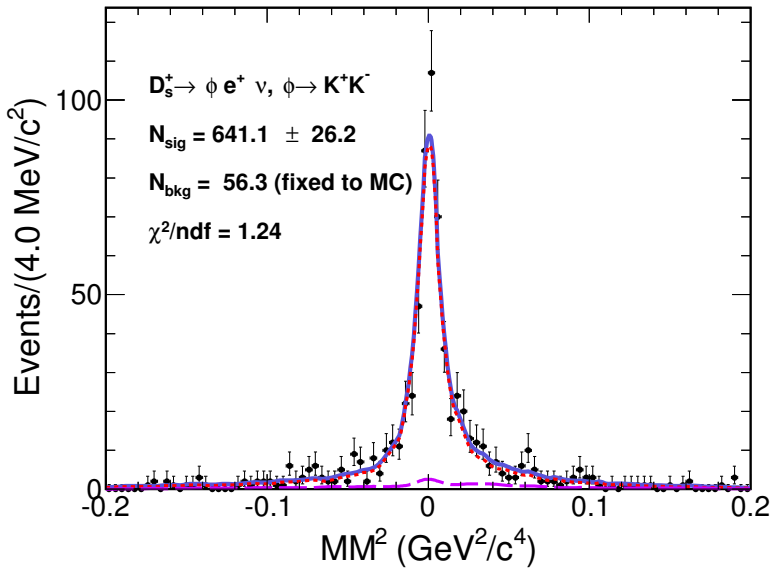

Figure 10: MM^2 fit to MC (round11). The points with error bars are generic MC, and the blue line is the fit. The red short-dashed line is signal; the violet long-dashed line is the background from generic MC. For the χ^2/ndf calculation, we merge the neighboring bins with a very few entries till there are 10 entries accumulated.

5.5 Systematic Uncertainties

The sources of systematic uncertainties on the branching fraction measurement are summarized in Table 8. We discuss each of them in the following in details. Note that most systematic uncertainties on the tag side cancel due to the double tag technique, so almost all the systematic uncertainties listed in the table apply only to the semileptonic side.

Table 8: The relative systematic uncertainties on the branching fraction measurement.

Source	$\mathcal{B}(D_s^+ \to \phi e^+ \nu_e)(\%)$
e^+ Tracking efficiency	0.5
e^+ PID efficiency	0.5
$K^\pm$ Tracking efficiency	2.0
$K^\pm$ PID efficiency	2.0
γ reconstruction	2.0
M^2_{rec} cut	1.2
K^+K^- Mass cut	0.7
Monto Carlo statistics	0.5
MM^2 fit	0.5
Background estimate	1.1
MC model	1.6
Tag yields	0.3
$\mathcal{B}(D_s^* \to \gamma D_s)$ & $\mathcal{B}(\phi \to K^+K^-)$	1.3
Total	4.1

- **$K^\pm$ Tracking/PID efficiency**

  By weighting our signal MC sample according to the systematic uncertainty of the momentum distribution which is based on the works [40, 41] by Xingyu Shan and Sanqiang Qu, etc, we obtain the uncertainties of $K^\pm$ tracking and PID efficiency which is close to 1.0%. To be conservative estimation, we sum their values as 2.0% for tracking and PID efficiencies.

- **e^+ Tracking/PID efficiency**

  We estimate these terms based on the systematic study from "the study of $D_s^+ \to \eta^{(\prime)} e^+ \nu_e$" [42]. In their memo, the discrepancies between data and MC are studied in each P_T (transverse momentum) vs $\cos(\theta)$ bin. The final uncertainties are evaluated with our signal MC sample using the weighted uncertainties, according to the $P_T : \cos(\theta)$ distribution. We find that these terms are both smaller than 0.5%. To be conservative, we assign 0.5% for e^+ tracking and PID.

- **γ reconstruction**

For the systematic uncertainty of photon reconstruction, it is safe to assign 2.0% from the study of "Systematic uncertainty of selecting the best photon candidate from $D_s^* \to \gamma D_s$ via the kinematic fit" [43] based on the same method, in which $D_s^+ \to K^+K^-\pi^+$ and $D_s^+ \to K_s^0K^+$ signal decay are used in the control sample.

- **M^2_{rec} cut**

  We vary this selection region by $\pm 20\,\mathrm{MeV}^2/c^4$ to obtain the new branching fraction measurements. By comparing to the nominal result with these new measurements, the largest difference 1.2% is taken as this systematic uncertainty.

- **K^+K^- Mass cut**

  We vary this selection region by $\pm 2\,\mathrm{MeV}/c^2$, which is about 6 times of the uncertainty of measured ϕ width, to obtain the new branching fraction measurements. The largest difference 0.7% is taken as this systematic uncertainty.

- **MC statistics**

  The uncertainty of MC statistics is obtained by $\sqrt{\sum_i (f_i \frac{\delta\epsilon_i}{\epsilon_i})^2}$, where f_i is the tag yield fraction and ϵ_i is the signal efficiency of tag mode i. We get 0.5% uncertainty for this term.

- **MM^2 fit**

  The uncertainty related to the MM^2 fit is estimated by varying the fitting range to (-0.18, 0.18)GeV^2/c^4 and (-0.22, 0.22)GeV^2/c^4. The largest difference 0.5% is taken as this systematic uncertainty.

- **Background estimate**

  For the generic background MC, we vary the yield of the peaking process $D_s^+ \to f_0(980)e^+\nu_e$, $f_0(980) \to K^+K^-$ by $\pm 1\sigma$ error and the yield of the contribution from $D_s^* \to D_s\pi^0$ by $\pm 1\sigma$ error according to PDG [20]. Since the main backgrounds from $D_sD_s^*$ process, we also consider the uncertainty from $D_sD_s^*$ cross section used in the generic MC and vary the background yield from $D_sD_s^*$ process by $\pm 1\sigma$ uncertainty corresponding to $\pm 1\sigma$ uncertainty of the measured $D_sD_s^*$ cross section [19]. Thus, we get these uncertainties and sum them in quadrature to be 1.1% as the uncertainty of the background estimate.

- **MC model**

  We vary the input of the form factor ratios r_V and r_2 according to the nominal solution by $\pm 1\sigma$ statistical error and generate the new signal MC samples to obtain the new branching fraction mea-

surement. Using the new signal shape and effiencies, the largest relative change of the branching fraction is 1.6%.

- **Tag yields**

  The uncertainty due to the tag yields is also considered. We vary the fitting range to [1.89, 2.04] GeV/c^2 and the background function to second-order chebyshev polynomial function, then the new tag yields lead to 0.07% and 0.30% change to the branching fraction, respectively. They are summed up as the uncertainty of tag yields.

- $\mathcal{B}(D_s^* \to \gamma D_s)$ **and** $\mathcal{B}(\phi \to K^+K^-)$

  We consider the uncertainty from the branching fractions of the intermediate states D_s^* and ϕ. They are estimated to be $\delta\mathcal{B}/\mathcal{B}$, 0.75% and 1.0%, respectively, according to PDG. We sum them up as the uncertainty due to the quoted branching fractions of intermediate states.

6 Partial Wave Analysis

After applying all the selection criterion described in Sec. 4.1 and Sec. 4.2, we require $3.78 < M^2_{\rm rec} < 4.05$ GeV$^2/c^4$, Mass(K^+K^-) < 1.08 GeV/c^2, and $|MM^2| < 0.06$ GeV$^2/c^4$ on the dataset to study the K^+K^- system and measure the form factor. This leads to 604 events, with an estimated background level of $(5.2 \pm 0.9)\%$ for the final state $D_s^+ \to K^+K^-e^+\nu_e$. In the preivous study at BABAR experiment [15], they observed a small S-wave contribution, possibly associated with $f_0(980) \to K^+K^-$. Hence, in order to confirm it at BESIII experiment, we perform partial wave analysis (PWA) for the D_s meson 4-body semileptonic decay (D_{e4}) to measure the form factors and the fractions of different components. The amplitude analysis method and the fitting solution are discussed in this section.

6.1 $D_s^+ \to K^+\ K^-\ e^+\ \nu_e$ decay rate parameterization

6.1.1 Kinematics and decay rate formalism

The 4-body decay $D_s^+ \to K^+K^-e^+\nu_e$ can be uniquely described by the 5 kinematic variables [44, 45] illustrated in Fig. 11: K^+K^- mass square (m^2), $e^+\nu_e$ mass square (q^2), the angle between the K^- three-momentum in the K^+K^- rest frame and the line of flight of the K^+K^- system in the D_s^+ rest frame (θ_K), the angle between the e^+ three-momentum in the $e^+\nu_e$ rest frame and the line of flight of the $e^+\nu_e$ system in the D_s^+ rest frame (θ_e), and the angle between the two decay planes (χ). The ranges of the three angular variables are $0 \le \theta_{K^+} \le \pi$, $0 \le \theta_e \le \pi$, $-\pi \le \chi \le \pi$. The sign of χ should be changed when analyzing D_s^- in order to keep CP conservation.

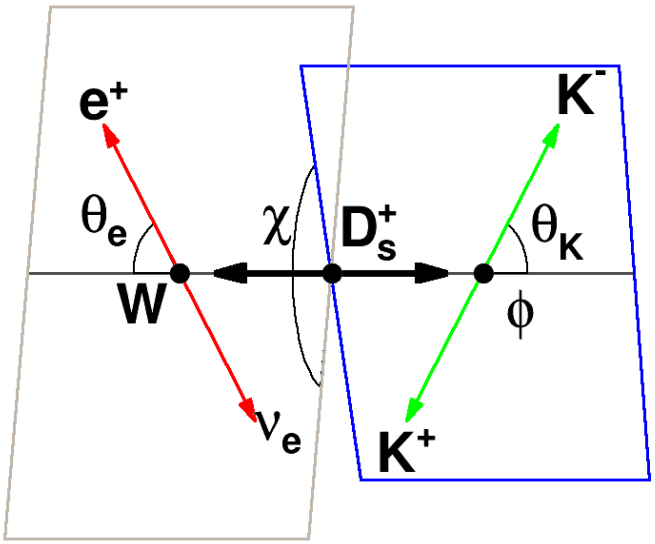

Figure 11: Definition of angular variables.

Based on the variables described above, the differential decay width for D_{e4} decay can be formalized in the kinematic region [46]. The whole formalism can be decomposed into form factors in representation of contributions from S, P and D waves. Neglecting the mass of electron or positron, we get the differential decay partial width as below:

$$d^5\Gamma = \frac{G_F^2||V_{cs}||^2}{(4\pi)^6 m_{D_s}^3} X\beta\mathcal{I}(m^2, q^2, \theta_{K^-}, \theta_e, \chi) \times dm^2 dq^2 dcos(\theta_{K^-}) dcos(\theta_e) d\chi. \tag{10}$$

In this expression, $X = p_{K^+K^-} m_{D_s}$, where $p_{K^+K^-}$ is the momentum of K^+K^- in the D_s rest frame, and $\beta = 2p^*/m$, in which p^* is the momentum of K^- in the K^+K^- rest frame. $\mathcal{I}$ is the decay intensity, which can be decomposed by θ_e and χ (Its form is quoted from [46] by default):

$$\begin{aligned}\mathcal{I} =& \mathcal{I}_1 + \mathcal{I}_2 cos2\theta_e + \mathcal{I}_3 sin^2\theta_e cos2\chi + \mathcal{I}_4 sin2\theta_e cos\chi + \mathcal{I}_5 sin\theta_e cos\chi \\ &+ \mathcal{I}_6 cos\theta_e + \mathcal{I}_7 sin\theta_e sin\chi + \mathcal{I}_8 sin2\theta_e sin\chi + \mathcal{I}_9 sin^2\theta_e sin2\chi,\end{aligned} \tag{11}$$

where $\mathcal{I}_{1,\ldots,9}$ depend on m^2, q^2 and θ_{K^-}. These quantities can be expressed in terms of the three form factors $\mathcal{F}_{1,2,3}$:

$$\begin{aligned}\mathcal{I}_1 =& \frac{1}{4}\{|\mathcal{F}_1|^2 + \frac{3}{2} sin^2\theta_{K^-}(|\mathcal{F}_2|^2 + |\mathcal{F}_3|^2)\}, \\ \mathcal{I}_2 =& -\frac{1}{4}\{|\mathcal{F}_1|^2 - \frac{1}{2} sin^2\theta_{K^-}(|\mathcal{F}_2|^2 + |\mathcal{F}_3|^2)\}, \\ \mathcal{I}_3 =& -\frac{1}{4}\{|\mathcal{F}_2|^2 - |\mathcal{F}_3|^2\} sin^2\theta_{K^-}, \\ \mathcal{I}_4 =& \frac{1}{2} Re(\mathcal{F}_1^* \mathcal{F}_2) sin\theta_{K^-}, \\ \mathcal{I}_5 =& Re(\mathcal{F}_1^* \mathcal{F}_3) sin\theta_{K^-}, \\ \mathcal{I}_6 =& Re(\mathcal{F}_2^* \mathcal{F}_3) sin^2\theta_{K^-}, \\ \mathcal{I}_7 =& Im(\mathcal{F}_1 \mathcal{F}_2^*) sin\theta_{K^-}, \\ \mathcal{I}_8 =& \frac{1}{2} Im(\mathcal{F}_1 \mathcal{F}_3^*) sin\theta_{K^-}, \\ \mathcal{I}_9 =& -\frac{1}{2} Im(\mathcal{F}_2 \mathcal{F}_3^*) sin^2\theta_{K^-}.\end{aligned} \tag{12}$$

Then form factors $\mathcal{F}_i$ can be expanded into partial waves to show their explicit dependence on θ_{K^-}. If only S, P and D waves are kept, this gives:

$$\begin{aligned}\mathcal{F}_1 &= \mathcal{F}_{10} + \mathcal{F}_{11} cos\theta_{K^-} + \mathcal{F}_{12} \frac{3cos^2\theta_{K^-} - 1}{2}, \\ \mathcal{F}_2 &= \frac{1}{\sqrt{2}}\mathcal{F}_{21} + \sqrt{\frac{3}{2}}\mathcal{F}_{22} cos\theta_{K^-}, \\ \mathcal{F}_3 &= \frac{1}{\sqrt{2}}\mathcal{F}_{31} + \sqrt{\frac{3}{2}}\mathcal{F}_{32} cos\theta_{K^-}.\end{aligned} \tag{13}$$

Here $\mathcal{F}_{i0}$, $\mathcal{F}_{i1}$ and $\mathcal{F}_{i2}$ correspond to S, P and D waves, respectively, of which we will provide the

specialized parameterization in the following sections. Since there is no D-waves to be considered in this analysis, the relevant terms of $\mathcal{F}_{i2}$ is zero.

6.1.2 P-wave form factor

P-wave related form factors $\mathcal{F}_{i1}$ can be parameterized by helicity form factors $H_{0,\pm}$:

$$\begin{aligned}\mathcal{F}_{11} =& 2\sqrt{2}\alpha q H_0 \times \mathcal{A}(m),\\ \mathcal{F}_{21} =& 2\alpha q (H_+ + H_-) \times \mathcal{A}(m),\\ \mathcal{F}_{31} =& 2\alpha q (H_+ - H_-) \times \mathcal{A}(m),\end{aligned} \tag{14}$$

where the α value is dependent on the definition of P-wave amplitude $\mathcal{A}(m)$, see Eq. 22. Then the helicity form factors can in turn be related to two axial-vector form factors $A_{1,2}(q^2)$ and one vector form factor $V(q^2)$:

$$\begin{aligned}H_0(q^2) &= \frac{1}{2mq}[(m_{D_s}^2 - m^2 - q^2)(m_{D_s}+m)A_1(q^2) - 4\frac{m_{D_s}^2 p_{K^+K^-}^2}{m_{D_s}+m}A_2(q^2)],\\ H_\pm(q^2) &= [(m_{D_s}+m)A_1(q^2) \mp \frac{2m_{D_s}p_{K^+K^-}}{(m_{D_s}+m)}V(q^2)].\end{aligned} \tag{15}$$

For the q^2 dependence we use a single-pole dominance parametrization (SPD):

$$\begin{aligned}V(q^2) &= \frac{V(0)}{1-\frac{q^2}{m_V^2}},\\ A_1(q^2) &= \frac{A_1(0)}{1-\frac{q^2}{m_A^2}},\\ A_2(q^2) &= \frac{A_2(0)}{1-\frac{q^2}{m_A^2}},\end{aligned} \tag{16}$$

where the pole mass m_V and m_A are expected to be close to $m_{D_s^*)} \backsimeq 2.1$ GeV/c^2 and $m_{D_{s1}} \backsimeq 2.5$ GeVc^2, respectively. The ratios of the form factors taken at $q^2 = 0$, $r_V = V(0)/A_1(0)$ and $r_2 = A_2(0)/A_1(0)$, can reflect the variation of the differential decay rate versus the kinematic variables. They are determined by fitting to the data. Then, the value of $A_1(0)$ can be calculated by combining the $D_s^+ \to \phi e^+ \nu_e$ branching fraction.

The amplitude $\mathcal{A}(m)$ for a specific resonance $\mathcal{R}$ is written as

$$\mathcal{A}(m) = \mathcal{R}(m) F_L(m), \tag{17}$$

where $\mathcal{R}(m)$ is the parameterization form to describe the resonance, L is angular momentum of K^+K^- system and

$$F_L = \left(\frac{p^*}{p_0^*}\right)^L \frac{B_L(p^*)}{B_L(p_0^*)}. \tag{18}$$

Here p^* is the momentum of the K^- in the K^+K^- rest frame, and p_0^* is the value taken at the pole mass of the resonance. B_L is the Blatt-Weisskopf damping factor [47] given by the following:

$$\begin{aligned} B_0 &= 1, \\ B_1 &= 1/\sqrt{1 + r_{BW}^2 p^{*2}}, \\ B_2 &= 1/\sqrt{(r_{BW}^2 p^{*2} - 3)^2 + 9 r_{BW}^2 p^{*2}}. \end{aligned} \tag{19}$$

where p^* is defined as in Eq. 18, and r_{BW} is the effective radius of the barrier in strong interaction for meson, which is poorly known. A common value of r_{BW} for light mesons is about 0.5 fm. Since this parameter is not sensitve in the PWA fit, we fix it at 3.0 GeV^{-1}. For vector meson ϕ, we use the relativistic Breit-Wigner (RBW) function to describe:

$$\mathcal{R}(m) = \text{RBW}(m) = \frac{m_0 \Gamma_0}{m_0^2 - m^2 - i m_0 \Gamma(m)}. \tag{20}$$

where m_0 and Γ_0 denote the pole mass and the total width of the resonance, respectively. As for the width $\Gamma(m)$, we use the following form:

$$\Gamma(m) = \Gamma_0 \left(\frac{p^*}{p_0^*}\right)^{2L+1} \left(\frac{m_0}{m}\right) \left(\frac{B_L(p^*)}{B_L(p_0^*)}\right)^2, \tag{21}$$

Here p^* and p_0^* are the same as in Eq. 18. In the case of ϕ, we can get $L = 1$. With the definition of the mass distribution given in Eq. 20, the factor α entering in Eq. 14 is equal to

$$\alpha = \sqrt{\frac{3\pi B_\phi}{p_0^* \Gamma_0}}, \tag{22}$$

where $B_\phi = \mathcal{B}(\phi \to K^+K^-)$.

6.1.3 S-wave form factor

In an S wave, only the helicity H_0 form factor can contribute, and we take the formalism used in BABAR experiment [48]:

$$F_{10} = p_{K^+K^-} m_{D_s} \frac{1}{1 - \frac{q^2}{m_A^2}} \mathcal{A}_S(m), \tag{23}$$

where $p_{K^+K^-}$ is the same as defined in X of Eq. 10. The term $\mathcal{A}_S(m)$ corresponds to the mass-dependent S-wave amplitude. We use the Flatté formula as employed for the $f_0(980)$ contribution,

$$\mathcal{A}_S(m) = \frac{a_S e^{i\phi_S}}{m_0^2 - m^2 - i(g_1 \rho_{\pi\pi} + g_2 \rho_{KK})}, \tag{24}$$

where a_S and ϕ_S are the magnitude and phase of the S-wave amplitude where they are measured comparing to the fixed ϕ; the parameters $g1$ and $g2$ are taken from Ref. [34]; the $\rho_{\pi\pi}$ and ρ_{KK} are the phase-space factors of the decay channels $\pi\pi$ and KK, respectively, which are defined as

$$\rho_{1,2}(m) = \sqrt{1 - 4\frac{m_{1,2}^2}{m}}, \qquad 1 \text{ and } 2 = \pi \text{ and } K. \tag{25}$$

6.2 Fit Method

We perform PWA fit using an unbinned maximum likelihood method in the RooFit framework. For one candidate event, the probability density function (PDF) can be expressed as:

$$PDF(\xi, \eta) = \frac{\omega(\xi, \eta)\epsilon(\xi)}{\int d\xi \omega(\xi, \eta)\epsilon(\xi)}, \tag{26}$$

where ξ denotes the final state of one event, and η denotes the parameters (need to be measured) in the PDF; $\omega(\xi, \eta)$ is the decay intensity (i.e., We define in Eq. 11), and $\epsilon(\xi)$ is the reconstruction efficiency for final state ξ. Then the likelihood is the product of probabilities of all the events:

$$\mathcal{L} = \prod_{i=1}^{N} PDF(\xi_i, \eta) = \prod_{i=1}^{N} \frac{\omega(\xi, \eta)\epsilon(\xi)}{\int d\xi \omega(\xi, \eta)\epsilon(\xi)}. \tag{27}$$

In the fit, we optimize the parameters η by performing a minimization of a negative log-likelihood (NLL):

$$-\ln\mathcal{L} = -\sum_{i=1}^{N} \ln(\epsilon(\xi_i)) - \sum_{i=1}^{N} \ln \frac{\omega(\xi, \eta)}{\int d\xi \omega(\xi, \eta)\epsilon(\xi)}. \tag{28}$$

The first term in Eq. 28 depends only on the events and efficiency, and remains constant during the fit. So actually we only compute the second term while performing the fit. Let σ_S be $\int d\xi \omega(\xi, \eta)\epsilon(\xi)$. we then minimize NLL:

$$NLL = -\sum_{i=1}^{N} \ln \frac{\omega(\xi_i, \eta)}{\sigma_S}. \tag{29}$$

The acceptance efficiency has been considered in the calculation of the cross section σ, which we calculate by making MC integration with signal MC (ie. DIY MC sample described in Sec. 3.2) [52]. The normalization integral terms can be given:

$$\sigma_S = \int d\xi \omega(\xi, \eta)\epsilon(\xi) \propto \frac{1}{N_{selected}} \sum_{k=1}^{N_{selected}} \frac{\omega(\xi_k, \eta)}{\omega(\xi_k, \eta_0)}. \tag{30}$$

Here the terms η and η_0 represent the value of the parameters used in the fit and those used to produce the simulated events, respectively. $N_{selected}$ denotes the number of the signal MC events after reconstruction and selection as described in Sec. 4.

The background is estimated by the generic MC in which the process $D_s^+ \to f_0(980)e^+\nu_e$, $f_0(980) \to K^+K^-$ is removed. They are subtracted from the total in the NLL calculation:

$$NLL = (-\ln\mathcal{L}_{data}) - w(-\ln\mathcal{L}_{bkg}), \tag{31}$$

where w is a normalized factor of the generic MC (40 rounds) corresponding to data size. We use all generic MC samples that is 40 times of data size and the normalized factor $w = 1/40$.

6.3 PWA Results

We perform a PWA fit to the $D_s^+ \to K^+K^-e^+\nu_e$ final state. The structure of K^+K^- system is dominated by the vector meson ϕ, and we also consider the possible K^+K^- S-wave from the $f_0(980)$. However, No significant excess is observed. So, we only consider ϕ in the K^+K^- system as the nominal solution. In the fit, the mass and width of ϕ are fixed to PDG values [20]. Then, we obtain the form factor values $r_V = V(0)/A_1(0) = 1.31 \pm 0.16 \pm 0.06$ and $r_2 = A_2(0)/A_1(0) = 0.76 \pm 0.17 \pm 0.05$, with a correlation coefficient $\rho_{r_V,r_2} = -0.26$, where the first errors are statistical and the second ones are systematic. The later ones are described in Sec. 6.5. The projections of five kinematic variables for this nominal fit result are shown in Fig. 12.

In addition, the possible $f_0(980)$ component as S-wave contribution to F_{10} term is studied by adding to the nominal solution, where $f_0(980)$ is parameterized by the Flatté formula and the paremeters are fixed based on the BES measurement [34]. The statistical significance of this component is determined to be less than 2σ from the change of $-2\ln\mathcal{L}$ in the PWA fits with and without this component, taking into account the change of the number of degrees of freedom. So no significant excess is found for this S-wave component. Besides, we also try to add a phase-space S-save amplitude to the nominal solution, and the significance is only about 2σ, so this contribution is also neglected.

6.4 Input and output check

In order to test the reliability of our fitting procedure, we generate 300 sets of toy MC samples, which include the signal MC $D_s^+ \to K^+K^-e^+\nu_e$ and the mixed backgrounds from generic MC samples. Each of them has similar statistics as data. For signal MC, they are generated by the amplitude formalism as Eq. 11 with the values of the parameters set to the nominal solution. Through event reconstruction, same selection criteria as done to data, we perfom the PWA fit to them and obtain the nominal solutions. The MC sample used for MC integration is also the same as that we use for data. For each fit result, we calculate the pull value $p = \frac{V_{fit}-V_{gen}}{\sigma_{fit}}$, where V_{gen} is the input value of the generator, and V_{fit} and σ_{fit} are the fitted value and its statistical uncertainty. These pull distributions behave as a normal Gaussian distribution and are fitted with a Gaussian function as shown in Fig. 13. In the fit of the pull distribution,

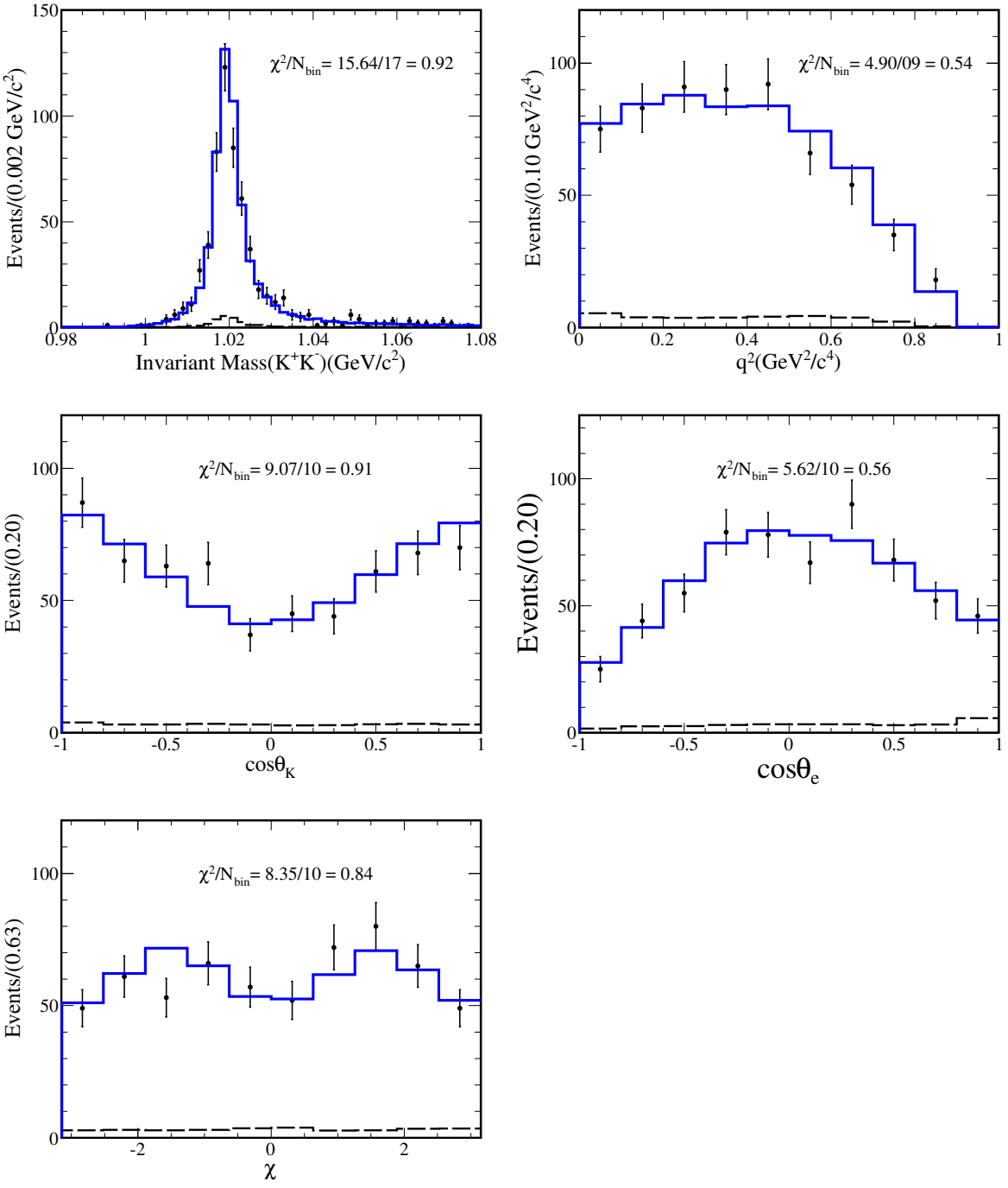

Figure 12: Projections of the data and PWA fit onto five kinematic variables for the $D_s^+ \to K^+K^-e^+\nu_e$ final state. The dots are data, the blue lines are fit, and the dashed lines show the sum of the background distributions from MC. For the $\chi^2/\mathrm{N_{bin}}$ calculation, we merge the neighboring bins with a very few entries till there are 10 entries accumulated.

the mean (μ) could give the bias from the fitting procedure, and the width (σ) could give the bias on the statistical uncertainty. We find that the fitting bias is negligible. In addition, we fix the mass and width of ϕ in the nominal fit. In order to confirm the rationality for these fixing, we perform another set of PWA fit with the mass and width floated besides the form factors in the fit. The results shown in Fig. 14 manifest that this dispose is adequate in the nominal fit.

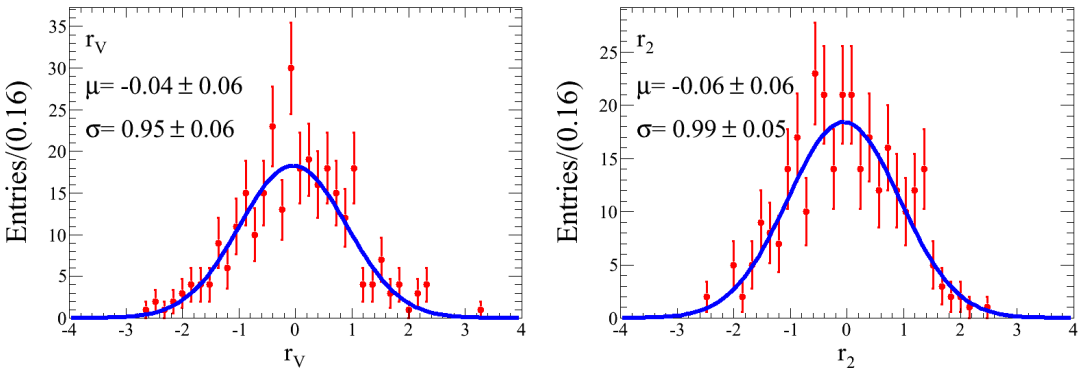

Figure 13: Fits to the pull distributions of the form factors (r_V, r_2) for the input-output check. The background is considered in the MC samples. The dots are MC, and the blue lines are the fits.

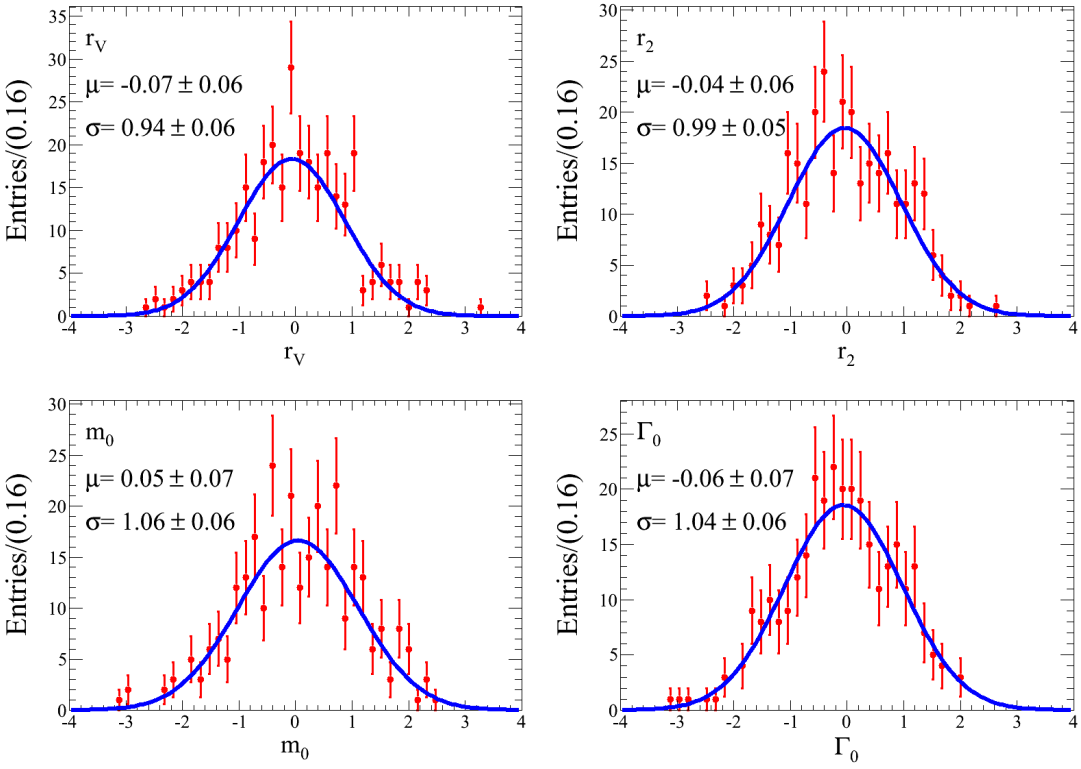

Figure 14: Fits to the pull distributions of the form factors (r_V, r_2), the mass and width of ϕ for the input-output check. The background is considered in the MC samples. The dots are MC, and the blue lines are the fits.

6.5 Systematic uncertainties

In this section, we consider the following sources of systematic uncertainty in the PWA fit, as summarized in Table. 9.

Table 9: Absolute systematic uncertainties (relative systematic uncertainties within the brackets) on the form factor ratios.

Source	r_V	r_2
$M^2_{\rm rec}$	0.031 (2.39%)	0.016 (2.10%)
MM^2	0.045 (3.44%)	0.027 (3.58%)
Background estimation	0.005 (0.35%)	0.034 (4.49%)
r_{BW}	0.003 (0.21%)	0.009 (1.15%)
m_V	0.011 (0.82%)	0.002 (0.31%)
m_A	0.012 (0.89%)	0.025 (3.27%)
ϕ line shape	0.0002 (0.02%)	0.0005 (0.07%)
MC scale factor	0.003 (0.25%)	0.004 (0.51%)
Total	0.06 (4.38%)	0.05 (7.05%)

- $M^2_{\rm rec}$ **and** MM^2

  We vary $M^2_{\rm rec}$ cut region by ± 0.02 GeV$^2/c^4$ and MM^2 cut region by ± 0.01 GeV$^2/c^4$. The largest difference compared to the nominal fit solution is taken as the uncertainty.

- **Background estimation**

  For this generic background MC, we add the contribution from the peaking process $D_s^+ \to f_0(980)e^+\nu_e$, $f_0(980) \to K^+K^-$ that is regenerated as described in Sec. 3.2, vary the background yield of the contribution from $D_s^* \to D_s\pi^0$ by $\pm 1\sigma$ error according to PDG [20] and the background yield from $D_sD_s^*$ process by $\pm 1\sigma$ uncertainty corresponding to $\pm 1\sigma$ uncertainty of the measured $D_sD_s^*$ cross secytion [19]. Then, we sum them with the largest difference in quadrature to be the uncertainty from background estimation.

- r_{BW}

  The effective radius of the resonance is set to 3.0 GeV^{-1} in the nominal fit. We vary this fixed value from 1.0 GeV^{-1} to 5.0 GeV^{-1}, and take the largest difference as systematic uncertainty due to the imperfect knowledge of this parameter.

- m_V **and** m_A

  We perform ± 100MeV$/c^2$ variation on m_V and m_A to estimate the uncertainties associated with

the pole mass assumption. The resulting differences compared to the nominal fit solution are taken as systematic uncertainties.

- **ϕ line shape**

  The mass and width of ϕ have been fixed at the PDG value [20]. We vary them $\pm 1\sigma$ within their central values, then the largest difference are taken as systematic uncertainties. We find they are very small and negligible.

- **MC scale factor**

  The uncertainty related to the scale factor of 40 times inclusive mc samples, which are used to model the background, is estimated by varying its value $\pm 10\%$. The largest difference are taken as systematic uncertainties.

7 Summary

In summary, we study the D_{e4} semileptonic decay of $D_s^+ \to K^+K^-e^+\nu_e$ based on 3.19 fb^{-1} of data sample recorded by the BESIII detector at BEPCII facility. This decay is dominated by the ϕ vector meson; we try to search for a K^+K^- S-wave contribtution, but no significant signal is found ($< 2\sigma$). By assuming only the ϕ contribution, we extract the form factor parameters from a fit to the five-dimensional decay distribution, assuming single-pole dominance parametrization, and obtain: $r_V = V(0)/A_1(0) = 1.31 \pm 0.16 \pm 0.06$ and $r_2 = A_2(0)/A_1(0) = 0.76 \pm 0.17 \pm 0.05$. We also measure the absolute branching fraction: $\mathcal{B}(D_s^+ \to \phi e^+\nu_e) = (2.31 \pm 0.10 \pm 0.09)\%$. These measurements are summaried in Table 10 and compared to the previous measurements and the theoretical calculations.

Our result of the form factors is consistent with FOCUS [18] measurement within the measured uncertainty, but has a quite tension on r_V compared to BABAR measurements [15] with more than 2.5σ deviation. Our form factor measurements are consistent with the theoretical predictions [7, 9, 10, 11, 12]. The check from experiment could improve our confidence in the determination of V_{cs} and the CKM unitarity test when the form factors are used as input from LQCD calculation.

Our branching fraction measurement is consistent with the previous measurements but closer to the result from CLEO [16]. It agrees well with CLF [12] and HQET [13], and it is also consistent with CUA [14] within 1.5σ experimental uncertainty. The difference compared to the newest result from CLF [11] is more than 2σ both considering the uncertainties from experiment and theory. It is also consistent with QCDSR [8], but the uncertainty from the theory is too large.

Table 10: Measured form factors and absolute branching fraction, compared with previous measurements.

Experiments	r_V	r_2	$\mathcal{B}(D_s^+ \to \phi e^+\nu_e)(\%)$
PDG2018 [53]	1.80±0.08	0.84±0.11	2.39 ± 0.16
this analysis	1.31±0.16±0.06	0.76±0.17±0.05	2.31 ± 0.10 ± 0.09
BABAR [15]	1.807±0.046±0.065	0.816±0.036±0.030	2.61 ± 0.03 ± 0.08 ± 0.15
CLEO [16]	–	–	2.36 ± 0.23 ± 0.13
CLEO [17]	–	–	2.14 ± 0.17 ± 0.08
FOCUS [18]	1.549±0.250±0.148	0.713±0.202±0.284	–
Theory			
LQCD [5]	$2.00\pm0.19^{+0.20}_{-0.25}$	$0.78\pm0.08^{+0.17}_{-0.13}$	–
LQCD [6]	2.01±0.04	0.68±0.07	–
LQCD [7]	1.72±0.21	0.74±0.12	–
QCDSR [8]	2.20±0.85	1.07±0.43	1.8 ± 0.5
CLF [9]	1.569	0.865	–
CLF [10, 11]	1.42	0.86	3.1 ± 0.3
CLF [12]	1.49	0.95	2.3
HQET [13]	1.80	0.52	2.4
CUA [14]	–	–	2.12

8 ChangLog

- Version 1.0 (August 24, 2018):

  Initial version for charm group convenors.

- Version 1.1 (September 8, 2018):

  In this version, we update the memo to response the comments from charm group convenor Hailong Ma. We mainly add more input-output check samples for the branching fraction measurement and the systematic uncertainty from tag yields. Many text descriptions are improved. The branching fraction value changes mainly due to a mistake of the signal efficiency calculation.

- Version 1.2 (November 15, 2018):

  In this version, we update the memo to mainly respond to the comments from charm group convenor Jim Libby, at the same time, the suggestons on text from Hailong are also considered. For the systematic uncertainties on BF, we do not use the information from tag D_s data sideband to estimate the background uncertainty since there are real D_s events under tag D_s mass.

- Version 1.3 (January 10, 2019):

  In this version, there is no much change compared to Version 1.2. We only make some modification about the mass windows seleciton at section 4.3.

- Version 1.4 (January 28, 2019):

  Based on the comments from our referee Peter Weidenkaff, we update the memo accordingly. The main changes are some text modification to clarify the analysis and removing the systematic uncertainties from the bias caused by the fitting procedure. The changes of our measurement results are negligible.

- Version 1.5 (March 20, 2019):

  In this version, we update the memo according to the comments from our referees Longke Li and Minggang Zhao. There are quite a lot improvement on text modification. We find a small mistake on MC truth count and update the single/double tag efficiencies as shown in Table 4 and Table 6. The largest change is from tag channel $D_s^- \to \pi^+\pi^-\pi^-$. The influence to our branch fraction measurement due to this change is negligible.

- Version 1.6 (August 30, 2019):

In this version, we update the memo according to the comments from our referees Longke and Peter. There is no change about the result.

- Version 2.0 (May 8, 2021):

  In this version, we update the BF and form factor measurement results. There is quite large change compared to the previous version. In the form factor measurement, we find a different solution with smaller NLL value. In the previous study, we used a set of initial value taken from BaBar [15] to perform the fit, consequently, a close result is obtained from the fit. To make more checks, we use the random values within the parameter range as the initial parameters to make 300 times of PWA fit, then a different solution turn out mostly, which is quite close to our final solution. To improve the result, we make several iterations for the PWA fit based on our method, i.e. generate the MC integral sample based the previous solution and use it to perform the PWA fit for the new solution, and circle till the difference is much less than 1%. Finally, the signal efficiency of the decay $D_s^+ \to \phi e^+ \nu_e$ is correspondingly updated to obtain the BF result.

References

[1] N. Cabibbo, Phys. Rev. Lett. **10**, 531 (1963);
M. Kobayashi and T. Maskawa, Prog. Theor. Phys. **49**, 652 (1973).

[2] M. Wirbel, B. Stech and M. Bauer, Z. Phys. C **29**, 637 (1985);
M. Bauer, B. Stech and M. Wirbel, Z. Phys. C **34**, 103 (1987);
N. Isgur, D. Scora, B. Grinstein, and M. B. Wise, Phys. Rev. D **39**, 799 (1989);
D. Scora and N. Isgur, Phys. Rev. D **52**, 2783 (1995);
D. Melikhov and B. Stech, Phys. Rev. D **62**, 014006 (2000);
T. Palmer and J. O. Eeg, Phys. Rev. D **89**, 034013 (2014);
N. R. Soni and J. N. Pandya, Phys. Rev. D **96**, 016017 (2017).

[3] A. Abada *et al.*, Nucl. Phys. B **619**, 565 (2001);
C. Aubin *et al.*, Phys. Rev. Lett. **94**, 011601 (2005);
H. Na *et al.*, Phys. Rev. D **82**, 114506 (2010);
H. Na *et al.*, Phys. Rev. D **84**, 114505 (2011);
S. Aoki *et al.*, (FLAG Working Group), Eur. Phys. J. C **77**, 112 (2017).

[4] M. A. Shifman, A. I. Vainshtein, and V. I. Zakharov, Nucl. Phys. B **147**, 385 (1979);
P. Ball, Phys. Rev. D **48**, 3190 (1993);
S. Narison, Nucl. Part. Phys. Proc. **258-259**, 189 (2015).

[5] C. Bernard, A. X. El-Khadra, and A. Soni, Phys. Rev. D **45**, 869 (1992).

[6] T. Bhattacharya and R. Gupta, Nucl. Phys. Proc. Suppl. **42**, 935 (1995).

[7] G. C. Donald, C. T. H. Davies, J. Koponen, and G. P. Lepage, (HPQCD Collaboration), Phys. Rev. D **90**, 074506 (2014).

[8] D. S. Du, J. W. Li, and M. Z. Yang, Eur. Phys. J. C **37**, 173 (2004).

[9] H. Y. Cheng, C. K. Chua, and C. W. Hwang, Phys. Rev. D **69**, 074025 (2004).

[10] R. C. Verma, J. Phys. G **39**, 025005 (2012).

[11] H. Y. Cheng and X. W. Kang, Eur. Phys. J. C **77**, 587 (2017).

[12] W. Wang and Y. L. Shen, Phys. Rev. D **78**, 054002 (2008).

[13] S. Fajfer and J. Kamenik, Phys. Rev. D **72**, 034029 (2005).

[14] T. Sekihara and E. Oset, Phys. Rev. D **92**, 054038 (2015).

[15] B. Aubert *et al.* (BABAR Collaboration), Phys. Rev. D **78**, 051101(R) (2008).

[16] K. M. Ecklund *et al.* (CLEO Collaboration), Phys. Rev. D **80**, 052009 (2009).

[17] K. M. Ecklund *et al.* (CLEO Collaboration), Phys. Rev. D **92**, 012009 (2015).

[18] B. Aubert *et al.* (FOCUS Collaboration), Phys. Lett. **B 586**, 183 (2004).

[19] D. Cronin-Hennessy *et al.* (CLEO Collaboration), Phys. Rev. D **80**, 072001 (2009).

[20] C. Patrignani *et al.* (Particle Data Group), Chin. Phys. C **40**, 100001 (2016).

[21] J. Adler *et al.* (MARK-III Collaboration), Phys. Rev. Lett. **62**, 1821 (1989).

[22] M. Ablikim *et al.* Nucl. Instrum. Meth. **A614**, 345 (2010).

[23] C. H. Yu *et al.* "BEPCII Performance and Beam Dynamics Studies on Luminosity", Proceedings of IPAC2016, Busan, Korea, 2016.

[24] X. Li *et al.*, Radiat. Detect. Technol. Methods **1**, 13 (2017); Y. X. Guo *et al.*, Radiat. Detect. Technol. Methods **1**, 15 (2017).

[25] Sangqiang Qu, Ke Liu, Minggang Zhao, and Hailong Ma, https://indico.ihep.ac.cn/event/7645/contribution/0/material/slides/0.pdf

[26] S. Agostinelli *et al.* (GEANT4 Collaboration), Nucl. Instrum. Meth. A **506**, 250 (2003).

[27] S. Jadach, B. F. L. Ward, and Z. Was, Phys. Rev. D **63**, 113009 (2001); Comput. Phys. Commun. **130**, 260 (2000).

[28] Ronggang Ping, BESIII Document/IHEP 162-v36.

[29] For the information about BesEvtGen and BesTwogam, please click here.

[30] D. J. Lange, Nucl. Instrum. Meth. A **462**, 152 (2001); R. G. Ping, Chin. Phys. C **32**, 599 (2008).

[31] J. C. Chen, G. S. Huang, X. R. Qi, D. H. Zhang, and Y. S. Zhu, Phys. Rev. D **62**, 034003 (2000); R. L. Yang, R. G. Ping, and H. Chen, Chin. Phys. Lett. **31**, 061301 (2014).

[32] E. Richter-Was, Phys. Lett. B **303**, 163 (1993).

[33] G. Balossini, C. M. Carloni Calame, G. Montagna, O. Nicrosini and F. Piccinini, Nucl. Phys. B **758**, 227 (2006); G. Balossini, C. Bignamini, C. M. C. Calame, G. Montagna, O. Nicrosini, and F. Piccinini, Phys. Lett. B **663**, 209 (2008).

[34] M. Ablikim *et al.* (BES Collaboration), Phys. Lett. **B 607**, 243 (2005).

[35] BESIII Document/HNU 867-v1.

[36] Lei Li, BESIII Document/BIPT 645-v20.

[37] Liu Chunlei,BESIII Document/CMU 123-v10.

[38] M. Ablikim *et al.* (BES Collaboration), Phys. Rev. D **72**, 092002 (2005).

[39] B. Aubert *et al.* (BABAR Collaboration), Phys. Rev. D **74**, 032003 (2006).

[40] https://indico.ihep.ac.cn/event/8006/contribution/1/material/slides/0.pdf

[41] https://indico.ihep.ac.cn/event/8023/contribution/1/material/slides/0.pdf

[42] Youhua Yang, BESIII Document/NJU 642-v30.

[43] http://indico.ihep.ac.cn/event/7187/contribution/1/material/slides/0.pdf

[44] N. Cabibbo and A. Maksymowicz, Phys. Rev. **137**, B438 (1965).

[45] A. Pais and S. B Treiman, Phys. Rev. **168**, 1858 (1968).

[46] C. L. Y. Lee, M. Lu, and M.B. Wise, Phys. Rev. D **46**, 5040 (1992).

[47] J. M. Blatt and V. F. Weisskopf, Theoretical Nuclear Physics, New YorK: John Wiley & Sons (1952); S. U. Chung *et al.*, Ann. Phys. **4**, 404 (1995).

[48] P. del Amo Sanchez *et al.* (BABAR Collaboration), Phys. Rev. D **83**, 072001 (2011).

[49] G. J. Gounaris and J. J. Sakurai, Phys. Rev. Lett. **21**, 244 (1968).

[50] R. R. Akhmetshin *et al.* (CMD-2 collaboration), Phys. Lett. **B 527**, 161 (2002).

[51] M. Ablikim *et al.* (BES Collaboration), Phys. Lett. **B 598**, 149-158 (2004).

[52] F.James, CERN 68-15 (1968).

[53] M. Tanabashi *et al.* (Particle Data Group), Phys. Rev. D **98**, 030001 (2018).